Discrete Energy-Conservation Properties in the Numerical Simulation of the Navier–Stokes Equations

Gennaro Coppola
Dipartimento di Ingegneria Industriale,
Università di Napoli "Federico II,"
Napoli 80125, Italy
e-mail: gcoppola@unina.it

Francesco Capuano
Dipartimento di Ingegneria Industriale,
Università di Napoli "Federico II,"
Napoli 80125, Italy
e-mail: francesco.capuano@unina.it

Luigi de Luca
Dipartimento di Ingegneria Industriale,
Università di Napoli "Federico II,"
Napoli 80125, Italy
e-mail: deluca@unina.it

Nonlinear convective terms pose the most critical issues when a numerical discretization of the Navier–Stokes equations is performed, especially at high Reynolds numbers. They are indeed responsible for a nonlinear instability arising from the amplification of aliasing errors that come from the evaluation of the products of two or more variables on a finite grid. The classical remedy to this difficulty has been the construction of difference schemes able to reproduce at a discrete level some of the fundamental symmetry properties of the Navier–Stokes equations. The invariant character of quadratic quantities such as global kinetic energy in inviscid incompressible flows is a particular symmetry, whose enforcement typically guarantees a sufficient control of aliasing errors that allows the fulfillment of long-time integration. In this paper, a survey of the most successful approaches developed in this field is presented. The incompressible and compressible cases are both covered, and treated separately, and the topics of spatial and temporal energy conservation are discussed. The theory and the ideas are exposed with full details in classical simplified numerical settings, and the extensions to more complex situations are also reviewed. The effectiveness of the illustrated approaches is documented by numerical simulations of canonical flows and by industrial flow computations taken from the literature. [DOI: 10.1115/1.4042820]

1 Introduction

Numerical discretizations of the Navier–Stokes (N–S) equations, especially for turbulent or high-Reynolds number flows, are frustratingly characterized by nonlinear instabilities arising from the approximation of the convective terms. This fact has been recognized since the first applications of numerical techniques for the solution of fluid flow equations [1]. In a series of seminal papers, the meteorological community clearly identified the problem and proposed various approaches for the resolution of this difficulty [2,3], leading the way to a rich field of research, which is still active nowadays [4,5].

The source of the instability, which cannot be alleviated by simply reducing the temporal mesh size, was identified in the accumulation of aliasing errors coming from the spatial discretization of the product of two or more variables in the nonlinear convective terms. Aliasing errors mainly occur because the nonlinear interaction of waves of certain frequencies can produce higher harmonics that lie outside the resolution range of the grid, and are thus "aliased" as long waves onto a resolved lower frequency. As such, the nonlinear instability has its origin mainly in the spatial discretization error of the convective nonlinear terms. In his landmark paper, Phillips [1] constructed a simple example, built upon a discretization of the vorticity equation for a two-dimensional (2D) flow in a channel, for which the nonlinear growth of aliased harmonics was analytically demonstrated. Since then, many evidences of this phenomenon have been documented for various nonlinear models and noteworthy for the N–S equations in three dimensions.

As a possible remedy, it was quickly recognized that a proper design of the spatial discretization procedure, able to preserve the integral constraints on quadratic quantities of physical importance, such as kinetic energy, greatly alleviated the instability, thus allowing the fulfillment of long-time integrations. Arakawa [6] was the first to show that it is possible to derive suitably discretized forms of the nonlinear convective term for which some quadratic invariants of the continuous equations can be preserved also at a discrete level. This procedure does not completely eliminate aliasing errors, which are still present and that typically manifest as a distortion of the energy spectrum. However, in many cases, the constraints on quadratic quantities force the solution to remain bounded, and permit to control aliasing errors in such a way that they do not affect the total energy of the system, eventually allowing stable simulations.

Since these first investigations, a remarkable number of studies have been devoted to the construction of numerical schemes, which are "physically consistent," in the sense that they are able to implicitly preserve some invariants or symmetries of the continuum equations. Kinetic energy-preserving numerical schemes based on the skew-symmetric splitting of convective derivatives are the most useful and the most studied among them, for both compressible and incompressible flows. In this review, some of the most successful ideas and approaches emerged over the last years in this field are presented, with emphasis on finite difference and finite volume simulations of turbulent flows, in the context of both direct and large-eddy simulation (LES) techniques.

The paper is organized as follows:[1] The conservation properties coming from spatial discretization, in the framework of the classical semidiscrete approach, are analyzed in Sec. 2. An introduction to most of the relevant theoretical concepts is presented in Sec. 2.1. In Secs. 2.2 and 2.3, the cases of incompressible and compressible flows are discussed separately, in view of some

Manuscript received July 2, 2018; final manuscript received February 8, 2019; published online March 6, 2019. Assoc. Editor: Sergei I. Chernyshenko.

[1]An earlier version of this paper was previously presented at the Italian conference AIMETA 2017, XXIII Conference of the Italian Association of Theoretical and Applied Mechanics [7]. In the present review, the original content has been improved and updated in many aspects, and the material has been overall reorganized. Most importantly, three new sections have been added, replacing and significantly enlarging the discussions on advanced topics and industrial applications and the number of cited references has almost doubled. Material that also appeared in Ref. [7] is reproduced here with permission.

fundamental differences between the two mathematical models. Since the focus of the paper lies on fundamental ideas and approaches, a significant part of the manuscript presents techniques applied to basic settings, under various simplifying assumptions. Extensions to more complex cases, as well as recent developments and further topics, are reviewed in Sec. 2.4. The topic of temporal conservation errors is then illustrated in Sec. 3, and the possibility to construct a numerical integration procedure able to preserve, at least approximately, quadratic invariants in time (a topic which has received growing interest in recent years) is discussed. The effectiveness of such approaches is documented by numerical simulations of canonical flows, which are reported throughout the text, while Sec. 4 presents some recent applications to *real-world* flows. Concluding remarks are finally given in Sec. 5.

2 Spatial Conservation

2.1 Theoretical Framework. In the context of the numerical discretization of the N–S equations, the topic of *spatial conservation* concerns the property of the semidiscretized formulations to reproduce the conservation symmetries of the continuous equations. Semidiscretization here stands for the usual numerical treatment in which the governing partial differential equations (PDEs) are first discretized in space, with the temporal variable left as continuous, and then integrated in time. The system of PDEs is hence first converted into a system of ordinary differential equations (ODEs); the integration in time is accomplished subsequently by employing dedicated solvers for the numerical integration of systems of ODEs. In this framework, it is desirable that in the spatial discretization step, the conservation symmetries of the continuous equations translate as suitably defined conservation symmetries of the system of ODEs. As it will be shown in the subsequent parts of this section, this target can be achieved only to a certain extent, and only in particular circumstances, whereas experience has shown that it is usually an important property for robustness and stability of the whole numerical integration process.

In this review, we will mainly focus on the treatment of the nonlinear convective terms of the N–S equations. The reason for this choice is that their nonlinearity is responsible for the production of aliasing errors, which are regarded as strongly harmful for stability and reliability of the numerical discretization. To fix the notations, and to introduce some of the important concepts, which will be recalled hereinafter, we consider the simple model equation

$$\frac{\partial \rho\varphi}{\partial t} = -\frac{\partial \rho u_j \varphi}{\partial x_j} \tag{1}$$

which expresses the balance of an extensive quantity per unit mass φ (ρ is the local density of the fluid) subject to convective fluxes due to a local velocity field with Cartesian components u_j. Both terms in Eq. (1) are present in the Euler and N–S equations for compressible and incompressible flows. In compressible flows, φ assumes the values unity, u_i or E for the balance of mass, momentum, and total energy, respectively. A similar structure is present also in the balance equations for entropy and internal energy, in which φ assumes the values s and e, respectively. In incompressible flows, ρ is constant in time and the continuity equation is recovered from Eq. (1) by setting $\rho = \text{constant}$ and $\varphi = 1$. Furthermore, the assumption $\rho = \text{constant}$ and $\varphi = u_i$ leads to the nonviscous balance equation for momentum, in which the pressure term is omitted.

Equation (1) has a *divergence structure*, which means that the rate of variation in time of the quantity $\rho\varphi$ is locally driven by the divergence of a flux vector. Application of the Gauss divergence theorem shows that this property implies that the integral of the quantity $\rho\varphi$ over an arbitrary domain depends only on the flux at the boundary. This circumstance is expressed by saying that the right-hand side of Eq. (1) has a *locally conservative* structure. Of course, this property implies that the quantity $\rho\varphi$ is also *globally conserved*, which means that the evolution of $\rho\varphi$ integrated over the entire domain depends only on the flux on the boundary. In other words, the total amount of the quantity inside the entire domain is conserved in the case of homogeneous or periodic boundary conditions. The variable associated with a globally conservative property is referred to as a linear invariant of Eq. (1).

By manipulating temporal and spatial derivatives (and by employing Eq. (1) in the case $\varphi = 1$), Eq. (1) easily leads to

$$\frac{\partial \rho\varphi^2/2}{\partial t} = -\frac{\partial \rho u_j \varphi^2/2}{\partial x_j} \tag{2}$$

which expresses the induced evolution equation for the generalized energy $\rho\varphi^2/2$. This equation shows that the divergence structure for the right-hand side of Eq. (1) induces a divergence structure for the generalized energy evolution equation. This in turn implies again that the global generalized energy (i.e., the total amount of generalized energy inside the domain) is conserved for periodic or homogeneous boundary conditions. In this case, the associated invariant is referred to as a quadratic invariant of Eq. (1).

In Euler and N–S equations, the evolution equation for each balanced quantity has a more complex structure, in which pressure and viscous terms can affect the conservation of quadratic invariants. However, in these cases, the considerations made above apply limited to the convective terms, which always have a structure of the type in Eq. (1). In these cases, we will refer to the above-mentioned property as the *globally energy preserving* character of the convective terms. In N–S equations total mass, total momentum (in absence of external forces) and total energy are easily shown to be linear invariants, whereas kinetic energy and helicity are quadratic invariants of incompressible Euler equations. Note that, on the other side, all the balanced quantities and all the associated generalized energies (i.e., all the quantities $\rho\varphi$ and $\rho\varphi^2/2$ with φ being unity, u_i, E, e or s) are globally preserved by convective terms.

When a semidiscretization procedure is applied to Eq. (1), the PDE reduces to a system of ordinary differential (or differential-algebraic) equations for a finite set of functions of time. The above-mentioned conservation properties of Eq. (1) are usually lost if discretization is not properly done, since discrete operators do not follow in general the standard rules of calculus. As an example, the so-called product rule for derivative, which is required to obtain Eq. (2) from Eq. (1), is typically not valid for discrete operators. There are several reasons to require that some fundamental conservation properties of the continuous equations are preserved upon spatial discretization. The divergence structure of the convective term of Eq. (1), for example, should be reproduced at a discrete level in compressible flows for the convergence to a weak solution in presence of discontinuities, while the global conservation of kinetic energy assures nonlinear stability in incompressible flows. The design of numerical spatial discretization procedures, which allow to preserve as much as possible conservation symmetries of the continuous equations, is the topic of this section.

In what follows, when a spatial discretization reproduces the divergence structure of Eq. (1), we will term it a *locally conservative* discretization. This is achieved when the discretization of the convective term at right-hand side of Eq. (1) can be cast as difference of fluxes at adjacent nodes. By application of the telescoping property, it is easily seen that discrete local conservation implies also discrete *global conservation*, i.e., the sum of all the fluxes on the mesh is zero for homogeneous or periodic boundary conditions, and the total amount of the species inside the domain is constant in time. This property is exactly the discrete reproduction of the preservation of the linear invariants of Eq. (1). The terminology related to quadratic invariants is similar: when a discretization reproduces the property that nonlinear terms, do not contribute to the discrete global energy balance; we will term it a *globally*

energy preserving discretization. *Local energy preserving* discretization is obtained, on the other side, in the particular case in which the spatial discretization of Eq. (1) is performed in such a way that in the induced discrete equation for the generalized energy convective terms can be cast as difference of fluxes at adjacent nodes for the variable $\rho\varphi^2/2$.

2.2 Incompressible Flows. Let us start with the incompressible N–S equations, which express the balance of mass and momentum for an homogeneous Newtonian fluid

$$\frac{\partial u_i}{\partial t}+\frac{\partial u_j u_i}{\partial x_j}=-\frac{\partial p}{\partial x_i}+\frac{1}{\mathrm{Re}}\frac{\partial^2 u_i}{\partial x_j \partial x_j} \tag{3}$$

$$\frac{\partial u_i}{\partial x_i}=0 \tag{4}$$

In these equations, which are written in nondimensional form, u_i and p are the (Cartesian) velocity components and the pressure, respectively, and $\mathrm{Re}=U_{\mathrm{ref}}L_{\mathrm{ref}}/\nu$ is the Reynolds number, ν being the kinematic viscosity. The system of equations Eqs. (3) and (4) constitutes a closed set of partial differential equations for the velocity components and the pressure, provided that suitable initial and boundary conditions are assigned. Note that in Eq. (3), the convective term has been written in its *divergence* form, as in Eq. (1). However, by analytically manipulating this term, and by employing the continuity equation Eq. (4), other forms are possible. Here, we mention the *advective* form, in which the nonlinear term is the product of transport velocity and the gradient of momentum, the *skew-symmetric* form, in which a mean value between advective and divergence forms is considered, and the *rotational* form, in which the cross product of vorticity and velocity appears. In summary, the following expressions have been considered:

$$(\mathrm{Div.})_i \equiv \frac{\partial u_j u_i}{\partial x_j} \tag{5}$$

$$(\mathrm{Adv.})_i \equiv u_j\frac{\partial u_i}{\partial x_j} \tag{6}$$

$$(\mathrm{Skew.})_i \equiv \frac{1}{2}\frac{\partial u_j u_i}{\partial x_j}+\frac{1}{2}u_j\frac{\partial u_i}{\partial x_j} \tag{7}$$

$$(\mathrm{Rot.})_i \equiv -u_j\left(\frac{\partial u_i}{\partial x_j}-\frac{\partial u_j}{\partial x_i}\right)-\frac{1}{2}\frac{\partial}{\partial x_i}u_j u_j \tag{8}$$

Actually, the nonlinear term can be written as any convex linear combination of two or more of these expressions, and still others are possible. This discussion has little importance in the context of the continuous equations, since the manipulations needed to switch from one to another are assumed to be always possible. This will be not the case for the discretized set of equations, since discrete operators do not follow in general the standard rules of calculus. This means that, while being equivalent on a continuous level, Eqs. (5)–(8) lead to different formulations when discretized. Hence, the way in which the nonlinear term is written has great importance once discretization is directly applied. Differences among the various formulations can have impact on stability, reliability, and quality of the numerical simulation.

The evolution of a number of physical quantities derived from velocity and pressure is governed by equations, which are obtained by analytical manipulation of Eqs. (3) and (4). The kinetic energy per unit mass $k=u_j u_j/2$, for example, evolves according to the following equation, which can be obtained by multiplying Eq. (3) by u_i and by employing Eq. (4):

$$\frac{\partial k}{\partial t}+\frac{\partial k u_j}{\partial x_j}+\frac{\partial T_j}{\partial x_j}=-\frac{2}{\mathrm{Re}}S_{ij}S_{ij} \tag{9}$$

where $T_j=u_j p-(2/\mathrm{Re})u_i S_{ij}$ and S_{ij} is the symmetric *rate of strain* tensor

$$S_{ij}=\frac{1}{2}\left(\frac{\partial u_i}{\partial x_j}+\frac{\partial u_j}{\partial x_i}\right) \tag{10}$$

Equation (9) is a derived equation, in the sense that it is not independent of mass and momentum balances. The evolution of kinetic energy can be uniquely determined once velocity and pressure evolutions in space and time are known, and it obeys Eq. (9), once a sufficient regularity of the solutions, which permits all the analytical manipulations, has been assumed.

The *global* kinetic energy, i.e., the total amount of kinetic energy contained in a given domain, evolves according to an equation which is simply derived by integrating both sides of Eq. (9) over the control volume Ω

$$\frac{\mathrm{d}K}{\mathrm{d}t}=-\int_\Omega\left(\frac{\partial k u_j}{\partial x_j}+\frac{\partial u_j p}{\partial x_j}-\frac{2}{\mathrm{Re}}\frac{\partial u_i S_{ij}}{\partial x_j}+\frac{2}{\mathrm{Re}}S_{ij}S_{ij}\right)\mathrm{d}\Omega, \tag{11}$$

where K is the integral of k over Ω. The first three terms at the right-hand side of Eq. (11) have a divergence structure, and by virtue of the Gauss divergence theorem, they are readily seen to contribute to the rate of change of K as surface integrals, thus accounting for inflow or outflow of kinetic energy by exchange of mass, or by pressure or viscous work. The last term is purely dissipative, and acts as a sink in the equation. For homogeneous or periodic boundary conditions, there is no way to exchange kinetic energy through the boundaries and the global kinetic energy equation reduces to

$$\frac{\mathrm{d}K}{\mathrm{d}t}=-\frac{2}{\mathrm{Re}}\int_\Omega S_{ij}S_{ij}\,\mathrm{d}\Omega \tag{12}$$

On the other hand, for general boundary conditions, and in absence of viscosity, global kinetic energy can neither be produced nor destroyed inside the volume and its rate of change depends only on what happens on the boundary. In the special case of a perfect fluid evolving in a domain with periodic or homogeneous boundary conditions, the total kinetic energy K remains constant during the evolution of the flow, i.e., it is a quadratic invariant of the incompressible Euler equations. We explicitly note that the divergence structure of the terms inside the integral has been obtained by manipulating the momentum equation and by making use of the continuity equation, which allows to rewrite, for instance, the pressure term $u_i\partial_i p$ as $\partial_i u_i p$.

2.2.1 Semidiscretization. We consider now the problem of numerical discretization of the system of N–S Eqs. (3) and (4). In this section, we will consider the problem of the *spatial* discretization, i.e., the discretization of the spatial domain and of the corresponding coordinates. The conservation properties of the discretization will be analyzed by considering the semidiscretized system of ODEs, and the ability of the spatial discretization to retain the invariant quantities of the continuous system. In what follows, we will mainly consider finite difference, finite volumes, or spectral discretizations on a Cartesian mesh, with uniform step size and periodic boundary conditions. This assumption is made here to allow a simpler discussion, but the extension to the cases of nonuniform meshes, curvilinear grids, and nonperiodic boundary conditions is in many cases straightforward, and is accomplished by considering the relevant scalar product associated with the metric. This extension is briefly considered in Sec. 2.4. The problem of the discretization on unstructured mesh is also recalled in Sec. 2.4.

Upon spatial discretization, the incompressible N–S equations can be expressed as

$$\frac{\mathrm{d}\mathbf{u}}{\mathrm{d}t}+\mathbf{C}(\mathbf{u})\mathbf{u}=-\mathbf{G}\mathbf{p}+\frac{1}{\mathrm{Re}}\mathbf{L}\mathbf{u} \tag{13}$$

$$\mathbf{Mu} = \mathbf{0} \tag{14}$$

where $\mathbf{u}$ is the discrete velocity vector containing the discretization of the components of velocity on the three-dimensional (3D) mesh, $\mathbf{u} = [\mathbf{u}_x\, \mathbf{u}_y\, \mathbf{u}_z]^{\mathrm{T}}$, the matrices $\mathbf{G} \in R^{N_\mathbf{u} \times N_p}$ and $\mathbf{M} \in R^{N_p \times N_\mathbf{u}}$ are the discrete gradient and divergence operators, respectively, while $\mathbf{L} \in R^{N_\mathbf{u} \times N_\mathbf{u}}$ is the block-diagonal Laplacian, $\mathrm{diag}(\mathfrak{L}, \mathfrak{L}, \mathfrak{L})$. $N_\mathbf{u}$ and N_p are the number of unknowns on the mesh for velocity and pressure, respectively. The gradient and divergence operators are assumed to be discretized consistently, in such a way that the relation $\mathbf{G}^{\mathrm{T}} = -\mathbf{M}$ holds. Temporal integration of the differential algebraic equation system (13) and (14) can be accomplished by formally recasting it as a system of ODE by enforcing the incompressibility constraint through the solution of the pressure Poisson's equation [8]. The details of the procedure are illustrated in Sec. 3.

The convective term can be expressed as the product of a linear block-diagonal convective operator $\mathbf{C}(\mathbf{u})$ and $\mathbf{u}$

$$\mathbf{C}(\mathbf{u})\mathbf{u} = \begin{bmatrix} \mathcal{C}_x(\mathbf{u}) & & \\ & \mathcal{C}_y(\mathbf{u}) & \\ & & \mathcal{C}_z(\mathbf{u}) \end{bmatrix} \begin{bmatrix} \mathbf{u}_x \\ \mathbf{u}_y \\ \mathbf{u}_z \end{bmatrix} \tag{15}$$

The operator $\mathbf{C}(\mathbf{u})$ is obtained by discretizing the nonlinear term starting from one of the possible expressions in which this can be written. As mentioned in Sec. 2.2, while all these expressions are equivalent in the continuous case, it is not so for the discrete equations. The generic matrix $\mathcal{C}_\times$, with $\times$ being x, y or z, assumes a specific form, which depends also on the details of the discretization, e.g., the way in which the variables are arranged on the mesh. It is well known that in problems in which systems of partial differential equations are discretized, it is sometimes advantageous to define discrete variables on different locations on the mesh. In that case, the discretization of nonlinear terms usually requires a strategy of interpolation of the different quantities, whose details influence the form of the discretized operator $\mathcal{C}_\times$.

The discrete quadratic conservation properties of the system (13) and (14) can be analyzed by deriving the evolution equation of the global discrete kinetic energy $\widehat{K}$. For uniform meshes, the scalar product is the discrete analog of integration and hence the discrete global kinetic energy per unit mass is simply $\widehat{K} = \mathbf{u}^{\mathrm{T}}\mathbf{u}/2$. Its evolution is governed by the equation:

$$\frac{\mathrm{d}\widehat{K}}{\mathrm{d}t} = -\mathbf{u}^{\mathrm{T}}\mathbf{C}(\mathbf{u})\mathbf{u} - \mathbf{u}^{\mathrm{T}}\mathbf{G}\mathbf{p} + \frac{1}{\mathrm{Re}}\mathbf{u}^{\mathrm{T}}\mathbf{L}\mathbf{u} \tag{16}$$

which is the discrete counterpart of Eq. (11). In Eq. (16), the pressure term contribution vanishes if $\mathbf{G}^{\mathrm{T}} = -\mathbf{M}$ and $\mathbf{Mu} = 0$, in the same way at it does in the continuous case. Note that this is true for *regular* or *staggered* arrangements of flow variables (using the terminology given in Ref. [9]), whereas pressure can contribute to the kinetic energy balance in *collocated* layouts as an error of order $\mathcal{O}(\Delta t^2 \Delta x^2)$ [10]. The diffusive term is the only physical contribution in Eq. (16) that correctly dissipates energy, being $\mathbf{L}$ a negative-definite matrix.

The convective term appears as a quadratic form with associated matrix $\mathbf{C}(\mathbf{u})$. Hence, this term does not contribute to the energy budget inside the domain if a skew-symmetric operator $\mathbf{C}(\mathbf{u})$ is adopted. This is the fundamental symmetry of the convective term that is associated with the conservation of global kinetic energy in the inviscid limit [11]. A discretization of the nonlinear term that is able to produce a skew-symmetric matrix $\mathbf{C}(\mathbf{u})$ for all $\mathbf{u}$ (or at least for all $\mathbf{u}$ satisfying $\mathbf{Mu} = 0$) is also such that it does not contribute to the global energy balance.

In subsequent sections, we will first analyze the *regular* layout of the variables, and then the *staggered* one.

2.2.2 Regular Layout. In this section, we will assume a *regular* layout of the flow variables, i.e., the case in which they are all defined on the same mesh location. In this case, the operators $\mathcal{C}$ do not depend on the particular direction, and can assume one of the following forms:

$$\mathcal{C}(\mathbf{u}) = \begin{cases} \mathcal{D} \equiv (\mathbf{D}_x\mathbf{U}_x + \mathbf{D}_y\mathbf{U}_y + \mathbf{D}_z\mathbf{U}_z) & Div, \quad (17a) \\ \mathcal{A} \equiv (\mathbf{U}_x\mathbf{D}_x + \mathbf{U}_y\mathbf{D}_y + \mathbf{U}_z\mathbf{D}_z) & Adv, \quad (17b) \\ \mathcal{S} \equiv \dfrac{1}{2}(\mathcal{A} + \mathcal{D}) & Skew. \quad (17c) \end{cases}$$

Note that the rotational form can instead be written as

$$\mathbf{C}(\mathbf{u}) = \mathbf{S}(\mathbf{R}\mathbf{u}) \tag{18}$$

where $\mathbf{S}$ is a skew-symmetric matrix performing pointwise vector product, and $\mathbf{R}$ is the (symmetric) curl operator, parentheses denoting functional dependence. In Eq. (17*a*), the square matrices $\mathbf{D}_\times$ represent the discrete derivative operators along each direction and acting on a whole set of scalar variables on the mesh, while $\mathbf{U}_\times$ are the diagonal matrices of the discretized velocity components along the three directions (e.g., $\mathbf{U}_x = \mathrm{diag}(\mathbf{u}_x)$). A first fundamental requirement for energy-preserving discretizations is that the derivative matrices derive from central schemes, which are free of numerical dissipation. In this case, on a uniform mesh, the matrices are skew-symmetric, i.e., $\mathbf{D}^{\mathrm{T}} = -\mathbf{D}$.[2] The aim here is to ensure that the convective term does not contribute to the global energy balance, Eq. (16). In a regular layout, the fulfillment of this target depends basically on the formulation employed for the convective term. It is easy to show from Eqs. (17*a*) to (17*b*) that the divergence and advective forms are associated with a convective operator, which is in general not skew-symmetric. In fact, they contribute to the total kinetic energy rate of variation with amounts, which are equal and of opposite signs. On the other side, from Eqs. (17*c*) to (18), it can be readily seen that the corresponding operator $\mathbf{C}(\mathbf{u})$ is skew-symmetric. As a consequence, only the skew-symmetric and the rotational forms of the convective term preserve energy spatially in the inviscid limit.

There has been a long debate regarding the use of the rotational or the skew-symmetric form [13,14]. While the rotational form is much more cost-effective than the skew-symmetric one (as discussed in more detail in Sec. 2.4), its aliasing errors are typically much higher. On the other hand, simulations carried out with the skew-symmetric form with or without dealiasing are typically very similar [15]. The skew-symmetric form is nowadays regularly applied in several highly accurate finite difference and spectral numerical codes for DNS and LES of turbulent flows [16,17].

[2]Note that for central-difference formulas, which lead to skew-symmetric derivative matrices, it can be readily shown that the integration-by-parts rule on periodic domains is still valid for discrete operators. This can be easily shown by employing the matrix notation. The integration-by-parts rule of the product of two functions u and v on a periodic domain (for which boundary terms cancel) can be written as

$$\int u\frac{\mathrm{d}v}{\mathrm{d}x}\,\mathrm{d}x = -\int v\frac{\mathrm{d}u}{\mathrm{d}x}\,\mathrm{d}x \tag{19}$$

The discrete formulation of the left-hand side of this equation on uniform periodic mesh is $\mathbf{u}^{\mathrm{T}}\mathbf{D}\mathbf{v}$, which is a scalar quantity. By transposing and applying the skew-symmetric property of $\mathbf{D}$, one has

$$\mathbf{u}^{\mathrm{T}}\mathbf{D}\mathbf{v} = \mathbf{v}^{\mathrm{T}}\mathbf{D}^{\mathrm{T}}\mathbf{u} = -\mathbf{v}^{\mathrm{T}}\mathbf{D}\mathbf{u} \tag{20}$$

which is the discrete analog of Eq. (19). Note that this property extends also to implicit spatial derivative schemes, for example to compact schemes [12]. In this last case, the derivative formula has the form: $\mathbf{A}\mathbf{u}' = \mathbf{B}\mathbf{u}$, where $\mathbf{A}$ is symmetric and $\mathbf{B}$ is skew-symmetric. Both $\mathbf{A}$ and $\mathbf{B}$ are circulant matrices for the case of periodic boundary conditions. Equation (20) assumes now the form

$$\mathbf{u}^{\mathrm{T}}\mathbf{A}^{-1}\mathbf{B}\mathbf{v} = \mathbf{v}^{\mathrm{T}}\mathbf{B}^{\mathrm{T}}\mathbf{A}^{-1^{\mathrm{T}}}\mathbf{u} = -\mathbf{v}^{\mathrm{T}}\mathbf{B}\mathbf{A}^{-1}\mathbf{u} = -\mathbf{v}^{\mathrm{T}}\mathbf{A}^{-1}\mathbf{B}\mathbf{u} \tag{21}$$

where the last equality holds because the matrices $\mathbf{A}^{-1}$ and $\mathbf{B}$ commute, being both circulant.

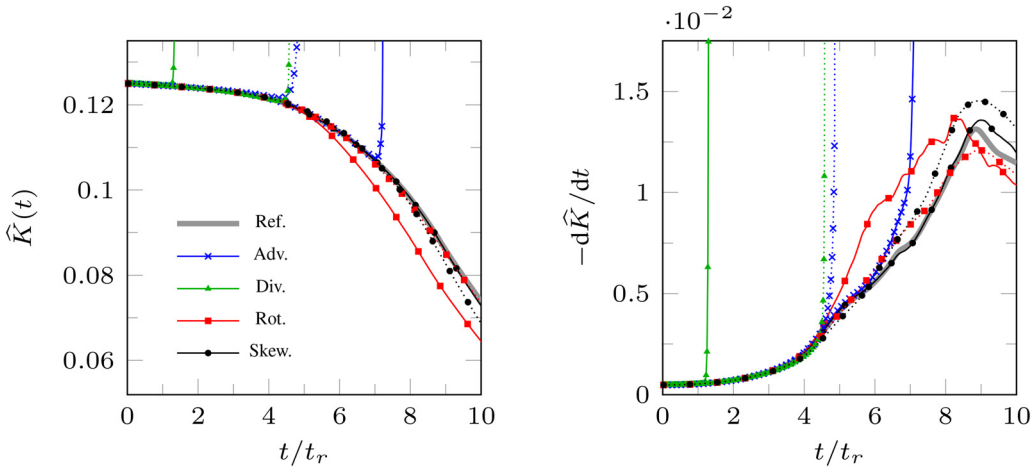

Fig. 1 Energy decay (left) and dissipation rate (right) for the TGV at Re = 1600 for second-order (dotted) and spectral (solid) accuracy on a 128^3 grid. The reference solution is a fully de-aliased computation with the same number of effective modes. The reference time is $t_r = L/U_0$.

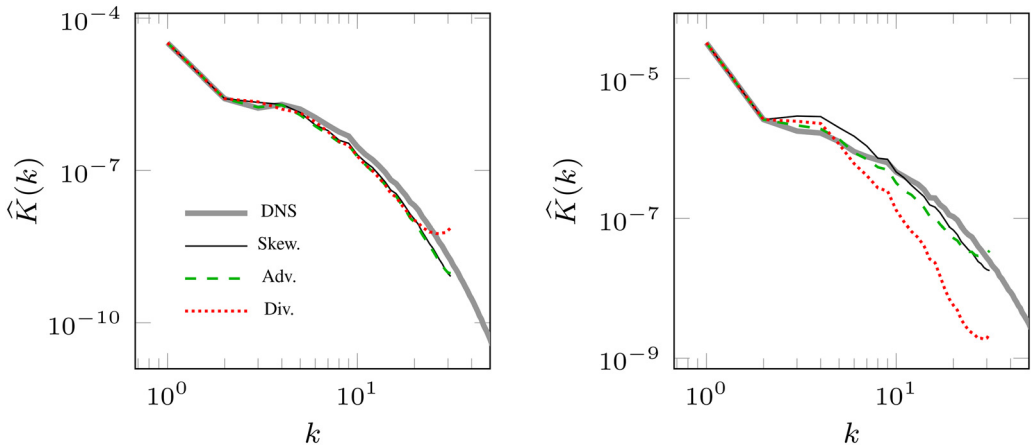

Fig. 2 Three-dimensional energy spectra for spectral large-eddy simulations of forced homogeneous isotropic turbulence at $\mathrm{Re}_\lambda = 100$ (left) and $\mathrm{Re}_\lambda = 170$ (right), using different formulations for the convective term. A reference direct numerical simulations (DNS) computation is also shown for comparison.

The conservation properties of the rotational form are also massively exploited [18,19].

The above considerations can be summarized by the following example. We consider the numerical integration of the three-dimensional Taylor-Green vortex (TGV), which is a canonical benchmark involving creation of small scales, transition to turbulence, and decay [20]. The initial conditions are prescribed in a triperiodic box of side $2\pi L$ and read

$$u(x,y,z,0) = U_0 \frac{2}{\sqrt{3}} \sin\left(\theta + \frac{2}{3}\pi\right) \sin(x)\cos(y)\cos(z) \tag{22}$$

$$v(x,y,z,0) = U_0 \frac{2}{\sqrt{3}} \sin\left(\theta - \frac{2}{3}\pi\right) \cos(x)\sin(y)\cos(z) \tag{23}$$

$$w(x,y,z,0) = U_0 \frac{2}{\sqrt{3}} \sin(\theta)\cos(x)\cos(y)\sin(z) \tag{24}$$

with $\theta = 0$ being used here. The TGV has been integrated on a 128^3 mesh by means of a pseudo-spectral method. Time integration is achieved by the standard fourth-order Runge–Kutta method (RK4) and a constant time-step, with CFL = 0.5. The various forms of the convective term mentioned earlier have been tested and compared in conjunction with both full spectral accuracy and second-order accuracy (the latter has been obtained by means of the modified-wavenumber approach). A reference solution has been obtained by using a de-aliasing procedure (2/3 rule [21]) and an equivalent number of effective modes. The selected Reynolds number is Re = 1600.

Results are shown in Fig. 1. The left figure shows the time evolution of the global energy, while in the right plot, the energy dissipation rate is reported. Due to the lack of discrete energy conservation, both the divergence and the advective formulations lead to a blow-up of the computation. On the other hand, the skew-symmetric and the rotational forms are stable in both the second-order and the spectral simulations. However, in the spectral case, the skew-symmetric form is much closer to the dealiased solution than the rotational form. This is due to the above-mentioned aliasing errors, which are higher for the rotational formulation. On the other hand, the difference is much less pronounced in the case of second-order simulations, due to the aliasing errors being *smoothed* by the truncation error of the difference scheme.

Energy conservation is not always only a matter of nonlinear stability. In some cases, computations might be stable due to concurrent effects (e.g., viscosity, external forcing), but eventually,

the results could be unreliable. For instance, Fig. 2 shows the three-dimensional energy spectra for spectral large-eddy simulations of forced homogeneous isotropic turbulence [22] at $\mathrm{Re}_\lambda = 100$ (left) and $\mathrm{Re}_\lambda = 170$ (right), using 64^3 grid points and the dynamic Smagorinsky model [23]. The forcing strategy is simply a freezing of the low wavenumbers ($||\mathbf{k}|| \leq 2$). An accompanying fully resolved DNS simulation is also shown for comparison. In this case, simulations are stable within the time integration interval (around 350 viscous time scales), but the energy spectra are significantly distorted for the advective and divergence formulations. Energy pile-up at high wavenumbers is clearly visible, while the divergence form at the highest Reynolds number has dissipated a large amount of the energy content.

2.2.3 Staggered Layout. The case of a staggered grid arrangement differs from the cases in which the variables are all defined at the same locations, essentially because the interpolation procedures needed to evaluate the different quantities at the same points add new degrees-of-freedom to the method. As a consequence, new possibilities arise of devising discretizations, which are energy conserving also for the divergence or advective forms. Of course, the whole operator $\mathbf{C}(\mathbf{u})$ still needs to be globally skew-symmetric, but this is achieved without necessarily employing the skew-symmetric form Eq. (17*c*).

In order to explain how this is achieved for a staggered mesh, the rest of the section focuses on the classical Harlow and Welch (H-W) scheme [24], with the aim of highlighting the above-mentioned points. The H-W procedure is very well suited for this analysis, since it is the simplest (second-order) and most used discretization procedure on staggered grids. It has a number of interesting properties, such as conservation of global kinetic energy. In line with Sec. 2.2.1, the discussion will be carried out by employing matrix notation.

The procedure starts by discretizing the variables on a Cartesian grid by collocating pressure nodes at the centers of the rectangular cells, while velocity component nodes at the face centers of each cell. The position and the indexing of the various variables are reported in Fig. 3 for the two-dimensional case, the three-dimensional extension being straightforward. Moreover, in constructing the one-dimensional arrays $\mathbf{u}$ and $\mathbf{p}$, we will assume that the variables on the two-dimensional mesh are sorted row-wise. Different conventions on the indexing and sorting of the variables are possible, and they would generate different multidimensional operators. However, the conclusions of the present analysis would remain unchanged.

For a staggered grid arrangement, in which each component of the velocity vector is defined on a different location, Eq. (16) gives the evolution of *one* possible definition of kinetic energy.

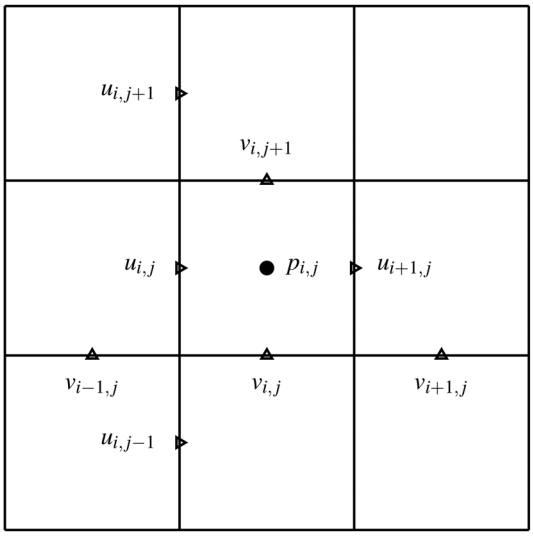

Fig. 3 Variables layout on a staggered mesh

More specifically, the quantity obtained by summing the squares of velocity components, each calculated on its location. Other definitions can be devised, which attempt to take into account the staggering of variables. As examples, a definition can be given in which each velocity component is suitably interpolated at cell centers before being squared and then summed, or the interpolation can be performed directly on the squares of velocity components. These definitions differ one from the other and the conservation properties also can be different. In order to avoid ambiguities, in what follows, we will first focus separately on the contributions to kinetic energy due to each single component of the velocity. The conservation properties of different definitions of total kinetic energy will be commented on at the end of this section.

For the case of the x component, for example, we will refer to $\widehat{K}_x = \mathbf{u}_x^{\mathrm{T}}\mathbf{u}_x/2$, for which we have the equation

$$\frac{\mathrm{d}\widehat{K}_x}{\mathrm{d}t} = -\mathbf{u}_x^{\mathrm{T}}\mathcal{C}_x(\mathbf{u})\mathbf{u}_x - \mathbf{u}_x^{\mathrm{T}}\mathbf{D}_x\mathbf{p} \tag{25}$$

in which the viscous term has been neglected. In this case, although the pressure contribution does not vanish (it should sum up to zero when added to the corresponding terms in the other directions), the convective term is still energy preserving if a skew-symmetric operator $\mathcal{C}_x$ is adopted.

The H-W procedure is based on a set of second-order derivative and interpolation schemes for which the differentiated or interpolated values on staggered locations are obtained by simple second-order formulas of the form

$$f_{i+1/2} = \frac{f_i + f_{i+1}}{2}, \quad f'_{i+1/2} = \frac{f_{i+1} - f_i}{h} \tag{26}$$

In order to express the convection matrix $\mathcal{C}_x$, the above operators have to be defined as matrix operators acting on the vectors of nodal values. If we consider a set of such nodal values on a uniform one-dimensional mesh with periodic boundary conditions: $\mathbf{f} = \{f_1, f_2 \ldots, f_N\}^{\mathrm{T}}$ with $f_{N+1} = f_1$, the basic linear operator on which derivative and interpolation matrices can be constructed is the shift operator $\mathbf{E}$, which is expressed as a circulant matrix given by

$$\mathbf{E} = \begin{bmatrix} 0 & 1 & 0 & \ldots & 0 \\ 0 & 0 & 1 & \ldots & 0 \\ \vdots & \vdots & \vdots & \cdots & \vdots \\ 0 & 0 & 0 & \ldots & 1 \\ 1 & 0 & 0 & \ldots & 0 \end{bmatrix} \tag{27}$$

The classical forward, backward, and central derivative matrices are defined as

$$\mathbf{D}^+ = \frac{\mathbf{E} - \mathbf{I}}{h}, \quad \mathbf{D}^- = \frac{\mathbf{I} - \mathbf{E}^{-1}}{h}, \quad \mathbf{D} = \frac{\mathbf{E} - \mathbf{E}^{-1}}{2h} \tag{28}$$

and in a similar manner, the forward and backward mean operators are defined

$$\mathbf{J}^+ = \frac{\mathbf{E} + \mathbf{I}}{2}, \quad \mathbf{J}^- = \frac{\mathbf{I} + \mathbf{E}^{-1}}{2} \tag{29}$$

For these operators, the following relations are easily proven:

$$(\mathbf{J}^+)^{\mathrm{T}} = \mathbf{J}^-, \quad (\mathbf{D}^+)^{\mathrm{T}} = -\mathbf{D}^-, \quad \mathbf{D}^-\mathbf{J}^+ = \mathbf{D}^+\mathbf{J}^- = \mathbf{D} \tag{30}$$

Moreover, hereinafter, we will use the following vectorial identity, which is valid for arbitrary vectors $\mathbf{u}$ and $\mathbf{v}$:

$$\mathbf{D}^-\mathbf{V}\mathbf{J}^+\mathbf{u} = \mathbf{J}^-\mathbf{V}\mathbf{D}^+\mathbf{u} + \mathbf{U}\mathbf{D}^-\mathbf{v} \tag{31}$$

where $\mathbf{U} = \mathrm{diag}(\mathbf{u})$ and $\mathbf{V} = \mathrm{diag}(\mathbf{v})$. Equation (31) can be written in equivalent forms as a matrix relation as follows:

$$\mathbf{D}^{-}\mathbf{U}\mathbf{J}^{+} = \mathbf{J}^{-}\mathbf{U}\mathbf{D}^{+} + \mathrm{diag}(\mathbf{D}^{-}\mathbf{u}) \tag{32}$$

$$\mathbf{D}^{-}\mathrm{diag}(\mathbf{J}^{+}\mathbf{u}) = \mathbf{J}^{-}\mathrm{diag}(\mathbf{D}^{+}\mathbf{u}) + \mathbf{U}\mathbf{D}^{-} \tag{33}$$

which are valid for all choices of $\mathbf{u}$. Equations (31)–(33) are all equivalent, and constitute a sort of "product rule" that is valid for the couple of differentiation-interpolation operators.

In multidimensional cases, the x- and y- direction shift operators are defined as

$$\mathbf{E}_x = \begin{bmatrix} \mathbf{E} & \mathbf{O} & \mathbf{O} & \dots & \mathbf{O} \\ \mathbf{O} & \mathbf{E} & \mathbf{O} & \dots & \mathbf{O} \\ \vdots & \vdots & \vdots & \cdots & \vdots \\ \mathbf{O} & \mathbf{O} & \mathbf{O} & \dots & \mathbf{E} \end{bmatrix}, \quad \mathbf{E}_y = \begin{bmatrix} \mathbf{O} & \mathbf{I} & \mathbf{O} & \dots & \mathbf{O} \\ \mathbf{O} & \mathbf{O} & \mathbf{I} & \dots & \mathbf{O} \\ \vdots & \vdots & \vdots & \cdots & \vdots \\ \mathbf{O} & \mathbf{O} & \dots & \mathbf{O} & \mathbf{I} \\ \mathbf{I} & \mathbf{O} & \dots & \mathbf{O} & \mathbf{O} \end{bmatrix} \tag{34}$$

where $\mathbf{O}$ is a suitable matrix with all entries equal to zero. Note that the matrix $\mathbf{E}_x$ is a $N_y \times N_y$ block matrix with blocks having dimensions $N_x \times N_x$, while the y-direction shift matrix $\mathbf{E}_y$ is a $N_x \times N_x$ block matrix with blocks having dimensions $N_y \times N_y$. The classical forward and backward derivative and interpolation matrices along the x directions are defined by

$$\mathbf{D}_x^{+} = \frac{\mathbf{E}_x - \mathbf{I}}{h}, \quad \mathbf{D}_x^{-} = \frac{\mathbf{I} - \mathbf{E}_x^{-1}}{h}, \qquad \mathbf{J}_x^{+} = \frac{\mathbf{E}_x + \mathbf{I}}{2}, \quad \mathbf{J}_x^{-} = \frac{\mathbf{I} + \mathbf{E}_x^{-1}}{2}, \tag{35}$$

and similarly for the y direction. It can be easily verified that relations analogous to Eq. (30) can be derived also for these multidimensional operators, provided that operators along the same direction are used. Equations (31)–(33) are still valid for multidimensional operators on each direction. Moreover, all the derivative and interpolation operators commute.

The discretization of the convective term by the H–W procedure can be expressed, by adopting the notation of Morinishi et al. [9], as

$$(\mathrm{Div.} - S2)_i = \frac{\widehat{\delta}_1 \overline{U_j}^{1x_i} \overline{U_i}^{1x_j}}{\widehat{\delta}_1 x_j} \tag{36}$$

The corresponding discretization of the continuity equation is

$$(\mathrm{Conv.} - S2) = \frac{\widehat{\delta}_1 U_i}{\widehat{\delta}_1 x_i} = 0 \tag{37}$$

In these last two equations, the operator $\widehat{\delta}_k$ is introduced, which is defined as the central difference with halved step size: $\widehat{\delta}_k f_j = f_{j+kh/2} - f_{j-kh/2}$. The overbar denotes a similarly defined interpolation operator.

In our notation, the continuity equation is given by

$$\mathbf{M}\mathbf{u} = \mathbf{D}_x^{+}\mathbf{u}_x + \mathbf{D}_y^{+}\mathbf{u}_y = 0 \tag{38}$$

while the x-momentum nonlinear term is

$$\mathcal{C}_x(\mathbf{u}) \cdot \mathbf{u}_x = (\mathbf{D}_x^{-}\mathrm{diag}(\mathbf{J}_x^{+}\mathbf{u}_x)\mathbf{J}_x^{+} + \mathbf{D}_y^{+}\mathrm{diag}(\mathbf{J}_x^{-}\mathbf{u}_y)\mathbf{J}_y^{-}) \cdot \mathbf{u}_x \tag{39}$$

By manipulating this expression and by making use of the commutative property of the Hadamard product $\mathrm{diag}(\mathbf{u})\mathbf{v} = \mathrm{diag}(\mathbf{v})\mathbf{u}$ and of the "product rule" (Eq. (33)) along each direction in the following forms:

$$\mathbf{D}_x^{-}\mathrm{diag}(\mathbf{J}_x^{+}\mathbf{u}_x) = \mathbf{J}_x^{-}\mathrm{diag}(\mathbf{D}_x^{+}\mathbf{u}_x) + \mathbf{U}\mathbf{D}_x^{-} \tag{40}$$

$$\mathbf{D}_y^{+}\mathrm{diag}(\mathbf{J}_y^{-}\mathbf{u}_x) = \mathbf{J}_y^{+}\mathrm{diag}(\mathbf{D}_y^{-}\mathbf{u}_x) + \mathbf{U}\mathbf{D}_y^{+} \tag{41}$$

one arrives to the expression

$$\begin{aligned} \mathcal{C}_x(\mathbf{u}) \cdot \mathbf{u}_x = {} & \mathbf{J}_x^{-}\mathrm{diag}(\mathbf{D}_x^{+}\mathbf{u}_x)\mathbf{J}_x^{+}\mathbf{u}_x + \\ & \mathbf{J}_y^{+}\mathrm{diag}(\mathbf{D}_y^{-}\mathbf{u}_x)\mathbf{J}_x^{-}\mathbf{u}_y + \\ & \mathbf{U}(\mathbf{D}_x^{-}\mathbf{J}_x^{+}\mathbf{u}_x + \mathbf{D}_y^{+}\mathbf{J}_x^{-}\mathbf{u}_y) \end{aligned} \tag{42}$$

The last term within the parentheses at the right-hand side of Eq. (42) can be rewritten by applying the commutative property of the products of derivative and interpolations matrices and by substituting $\mathbf{J}_x^{+}\mathbf{D}_x^{-} = \mathbf{J}_x^{-}\mathbf{D}_x^{+}$. It thus assumes the form

$$\mathbf{U}\mathbf{J}_x^{-}(\mathbf{D}_x^{+}\mathbf{u}_x + \mathbf{D}_y^{+}\mathbf{u}_y) \tag{43}$$

which vanishes by virtue of continuity equation Eq. (38). By applying again the commutative property of the Hadamard product to Eq. (39) and to the first two terms at the right-hand side of Eq. (42) one has the following two equivalent expressions for the matrix $\mathcal{C}_x$:

$$\mathcal{C}_x(\mathbf{u}) = \mathbf{D}_x^{-}\mathrm{diag}(\mathbf{J}_x^{+}\mathbf{u}_x)\mathbf{J}_x^{+} + \mathbf{D}_y^{+}\mathrm{diag}(\mathbf{J}_x^{-}\mathbf{u}_y)\mathbf{J}_y^{-} \tag{44}$$

$$\mathcal{C}_x(\mathbf{u}) = \mathbf{J}_x^{-}\mathrm{diag}(\mathbf{J}_x^{+}\mathbf{u}_x)\mathbf{D}_x^{+} + \mathbf{J}_y^{+}\mathrm{diag}(\mathbf{J}_x^{-}\mathbf{u}_y)\mathbf{D}_y^{-} \tag{45}$$

from which it is readily seen that one is the opposite of the transpose of the other, i.e., $\mathcal{C}_x = -(\mathcal{C}_x)^{\mathrm{T}}$, which shows that $\mathcal{C}_x$ is, in fact, skew-symmetric.

The skew-symmetry of the matrix $\mathcal{C}_x$ shows that the contribution of the convective term to the global quantity $\hat{K}_x$ vanishes. Since the sum of the pressure terms in Eq. (25) along the three directions vanishes by virtue of the continuity equation, the present analysis shows that the global kinetic energy defined as the sum of all the contributions along each direction, each calculated on its location, is conserved by the H–W scheme. This quantity can be expressed as $u_i u_i/2$, where summation over the repeated index is assumed. A different global kinetic energy can be defined by interpolating velocity components at cell centers before squaring and summing. In the notation of Morinishi et al. [9], this quantity can be written as: $\overline{u_i}^{1x_i}\overline{u_i}^{1x_i}/2$ while in our notation, it reads $(\mathbf{J}_x^{+}\mathbf{u}_x)^{\mathrm{T}}\mathbf{J}_x^{+}\mathbf{u}_x/2$. For this quantity, our analysis shows that the convective terms in the global kinetic energy balance contribute with the term $\mathbf{u}_x^{\mathrm{T}}\mathbf{J}^{-}\mathbf{J}^{+}\mathcal{C}_x(\mathbf{u})\mathbf{u}_x$, which does not vanish in general for skew-symmetric matrices $\mathcal{C}_x(\mathbf{u})$. This shows that the global kinetic energy calculated on interpolated velocity components is not conserved in general. A third form of global energy is defined by the quantity $\overline{u_i u_i}^{1x_i}/2$ [25], i.e., the one obtained by summing the interpolated velocity products. In our notation, this form of global kinetic energy along the direction x is defined as $\mathbf{1}^{\mathrm{T}}\mathbf{J}_x^{+}\mathbf{U}_x\mathbf{u}_x$, where $\mathbf{1}$ stands for the column vector of all terms equal to unity. The contribution of the convective term to the x-component global energy variation in time is $-\mathbf{1}^{\mathrm{T}}\mathbf{J}_x^{+}\mathbf{U}_x\mathcal{C}_x(\mathbf{u})\mathbf{u}_x$, which can be shown to be equal to $\mathbf{u}_x^{\mathrm{T}}\mathcal{C}_x(\mathbf{u})\mathbf{u}_x$ by employing the identity $\mathbf{U}_x\mathbf{J}^{-}\mathbf{1} = \mathbf{u}_x$, and hence vanishes for a skew-symmetric matrix $\mathcal{C}_x$. This shows that the convective term does not contribute to the evolution of the global kinetic energy for skew-symmetric convective operators, and is hence globally energy preserving for this form of kinetic energy. In the same fashion, the pressure term can be shown to vanish, provided the continuity equation is satisfied. This assures that kinetic energy obtained by interpolating the velocity products is globally conserved.

The H–W scheme has provided the basis for a number of successful discretizations that have been developed over the last decades. Extensions and refinements of the method are discussed in Sec. 2.4. Numerical tests employing the H–W method are shown in Sec. 3.

2.3 Compressible Flows. In the case of compressible flow models, since density is allowed to vary, the pressure has its full thermodynamic role, and its variations influence the density and

the temperature through an equation of state. In this case, the balance equations for mass and momentum do not constitute a closed set of equations alone, since the internal energy of the fluid influences pressure and density variations through the equation of state. As a consequence, the system of balance equations for a compressible flow includes an equation for internal or total energy as well as an equation of state. By choosing the total energy as the additional balanced quantity, the system of N–S equations for compressible flows reads

$$\frac{\partial \rho}{\partial t} = -\frac{\partial \rho u_j}{\partial x_j} \tag{46}$$

$$\frac{\partial \rho u_i}{\partial t} = -\frac{\partial \rho u_j u_i}{\partial x_j} - \frac{\partial p}{\partial x_i} + \frac{\partial \tau_{ij}}{\partial x_j} \tag{47}$$

$$\frac{\partial \rho E}{\partial t} = -\frac{\partial \rho u_j E}{\partial x_j} - \frac{\partial p u_j}{\partial x_j} + \frac{\partial \tau_{ij} u_i}{\partial x_j} + \frac{\partial}{\partial x_j}\left(\kappa \frac{\partial T}{\partial x_j}\right) \tag{48}$$

where T is the temperature, κ is the thermal conductivity, and ρE is the total energy per unit volume, being $E = u_i u_i/2 + e$ where $e = c_v T$ is the internal energy per unit mass and c_v is the specific heat at constant volume. The stress tensor is obtained by the usual relation

$$\tau_{ij} = \mu\left(\frac{\partial u_i}{\partial x_j} + \frac{\partial u_j}{\partial x_i}\right) - \frac{2}{3}\mu \frac{\partial u_k}{\partial x_k}\delta_{ij} \tag{49}$$

where μ is the molecular viscosity and δ_{ij} is the identity tensor. Closure is achieved by the ideal equation of state $p = \rho RT$, with R the universal gas constant.

The nonlinear convective terms in Eqs. (46)–(48) share the common structure of the right hand side of Eq. (1)

$$\mathcal{C} = \frac{\partial \rho u_j \varphi}{\partial x_j} \tag{50}$$

where φ equals one, u_i and E for the mass, momentum, and energy terms, respectively. As for incompressible flows, in a continuous setting, the convective terms can be expressed in several analytically equivalent forms. However, the generic nonlinear terms in momentum and energy equations have a cubic nonlinearity, and hence the number of basic forms in which they can be expressed by applying the product rule raises from two (divergence and advective) to five (one of divergence- and four of advective-type), which are listed as follows:

$$\mathcal{C}^D = \frac{\partial \rho u_j \varphi}{\partial x_j} \tag{51}$$

$$\mathcal{C}^u = u_j \frac{\partial \rho \varphi}{\partial x_j} + \rho \varphi \frac{\partial u_j}{\partial x_j} \tag{52}$$

$$\mathcal{C}^\varphi = \varphi \frac{\partial \rho u_j}{\partial x_j} + \rho u_j \frac{\partial \varphi}{\partial x_j} \tag{53}$$

$$\mathcal{C}^\rho = \rho \frac{\partial u_j \varphi}{\partial x_j} + \varphi u_j \frac{\partial \rho}{\partial x_j} \tag{54}$$

$$\mathcal{C}^L = \rho \varphi \frac{\partial u_j}{\partial x_j} + \rho u_j \frac{\partial \varphi}{\partial x_j} + \varphi u_j \frac{\partial \rho}{\partial x_j} \tag{55}$$

The terms appearing in Eqs. (51)–(55) deserve some discussion. Equation (51) is the usual divergence form, while Eqs. (52) and (53) were introduced by Blaisdell et al. [14] and Feiereisen et al. [26], respectively, who were the first to use these forms, in conjunction with $\mathcal{C}^D$, to obtain stable simulations, as it will be discussed in the following. As for the remaining forms, discretization of Eq. (54) was considered for the first time by Kennedy and Gruber [27], while the one in Eq. (55) is named *linear* since only the gradients of linear quantities appear. Note that for the continuity equation, the forms $\mathcal{C}^D$ and $\mathcal{C}^\varphi$ reduce to the classical divergence form, while $\mathcal{C}^u$, $\mathcal{C}^\rho$, and $\mathcal{C}^L$ are equivalent to the unique advective form, which can be defined for the case of quadratic nonlinearities.

As already observed for the incompressible flow equations, any linear convex combination of the above-mentioned forms can be equally considered as a consistent expression of the nonlinear convective term. This distinction has again little importance in the continuous formulation, since all these expressions are equivalent once the analytical manipulations required to derive one from the others are assumed to be valid. However, the corresponding discretizations behave usually differently, because the product rule, which is required to switch from one form to the others, is in general not valid.

Note that Eq. (48) can be replaced by the equation for internal energy ρe

$$\frac{\partial \rho e}{\partial t} = -\frac{\partial \rho u_j e}{\partial x_j} - p\frac{\partial u_j}{\partial x_j} + \tau_{ij}\frac{\partial u_i}{\partial x_j} + \frac{\partial}{\partial x_j}\left(\kappa \frac{\partial T}{\partial x_j}\right) \tag{56}$$

or by the entropy equation

$$\frac{\partial \rho s}{\partial t} = -\frac{\partial \rho u_j s}{\partial x_j} + \frac{1}{T}\left[\tau_{ij}\frac{\partial u_i}{\partial x_j} + \frac{\partial}{\partial x_j}\left(\kappa \frac{\partial T}{\partial x_j}\right)\right] \tag{57}$$

where s is given by the relation $s = c_v \ln(p/\rho^\gamma)$ and $\gamma = c_p/c_v$ with c_p specific heat at constant pressure.

2.3.1 Kinetic Energy Equation. The induced evolution equation for the kinetic energy $\rho k = \rho u_i u_i/2$ can be derived by starting from the following relation, which is obtained by manipulating only temporal derivatives:

$$\frac{\partial \rho k}{\partial t} = u_i \frac{\partial \rho u_i}{\partial t} - \frac{u_i u_i}{2}\frac{\partial \rho}{\partial t} \tag{58}$$

By substituting the right-hand side of Eqs. (46) and (47) (in the inviscid limit) into Eq. (58), regardless of the choice made for the convective terms formulation, in a continuous setting, Eq. (58) can be easily shown to assume the form

$$\frac{\partial \rho k}{\partial t} = -\frac{\partial \rho u_j k}{\partial x_j} - u_j \frac{\partial p}{\partial x_j} \tag{59}$$

from which it is evident that, as expected, the nonlinear convective term in the kinetic energy equation has a divergence structure. Hence, it does not contribute to *global* energy evolution, i.e., to the evolution of kinetic energy integrated over the whole domain, provided that periodic or homogeneous boundary conditions are applied. Note that, in contrast to what happens in the incompressible limit, the global kinetic energy is not an invariant of the inviscid equations since isentropic exchanges of kinetic and internal energy are allowed through the work done by the pressure term.

The derivation of Eq. (59) from Eq. (58) employs the classical product rule for derivatives, which is generally violated by discrete operators. As a consequence, the analytically equivalent forms, Eqs. (51)–(55), behave differently when discretized, and the divergence structure of the convective term in Eq. (59) is in general not reproduced at a discrete level by the numerical approximation. The idea, which has been pursued over the past years, in analogy with the approaches, which proved to be successful in the incompressible case, relies on the possibility to construct a suitable linear combination of two (or more) discretized forms among Eqs. (51)–(55), in such a way that the nonlinear term does not spuriously contribute to the global energy balance. In other words, the integral of the convective term over the

domain should vanish for periodic or homogeneous flux boundary conditions, similarly to what happens in Eq. (59). These forms have been termed as "skew-symmetric" forms, although strictly speaking, as also observed by Pirozzoli [28], the differential operator relative to a single variable φ is not skew-symmetric. However, as it will be shown in the following, the application of these "skew-symmetric" forms in both continuity and momentum equations can produce an energy-preserving discretization in which the convective term in the induced discrete kinetic energy equation does not spuriously contribute to the global energy production.

As already mentioned above, the classical forms, which has been first proposed and applied in the literature are the Feiereisen et al. form [26], in which the following splitting is adopted:

$$\frac{\partial \rho u_j \varphi}{\partial x_j} \rightarrow \frac{1}{2}\frac{\partial \rho u_j \varphi}{\partial x_j} + \frac{1}{2}\left(\varphi \frac{\partial \rho u_j}{\partial x_j} + \rho u_j \frac{\partial \varphi}{\partial x_j}\right) \tag{60}$$

and the Blaisdell et al. form [14]

$$\frac{\partial \rho u_j \varphi}{\partial x_j} \rightarrow \frac{1}{2}\frac{\partial \rho u_j \varphi}{\partial x_j} + \frac{1}{2}\left(\rho\varphi \frac{\partial u_j}{\partial x_j} + u_j \frac{\partial \rho \varphi}{\partial x_j}\right) \tag{61}$$

The first form was derived in strict analogy with the skew-symmetric form in the incompressible case, and was shown to be energy preserving when applied to both continuity and momentum equations. The second one, on the other hand, was proposed as a result of a study on the minimization of aliasing errors and it can be shown to be not strictly energy preserving.

To show energy preservation of the Feiereisen form, one can write down the continuity and momentum equations split with this form, which are

$$\frac{\partial \rho}{\partial t} = -\frac{\partial \rho u_j}{\partial x_j} \tag{62}$$

$$\frac{\partial \rho u_i}{\partial t} = -\frac{1}{2}\left(\frac{\partial \rho u_j u_i}{\partial x_j} + u_i \frac{\partial \rho u_j}{\partial x_j} + \rho u_j \frac{\partial u_i}{\partial x_j}\right) - \frac{\partial p}{\partial x_i} \tag{63}$$

and substitute these expressions into Eq. (58)

$$\frac{\partial \rho k}{\partial t} = -\frac{1}{2}u_i\left(\frac{\partial \rho u_j u_i}{\partial x_j} + u_i \frac{\partial \rho u_j}{\partial x_j} + \rho u_j \frac{\partial u_i}{\partial x_j}\right) - u_i \frac{\partial p}{\partial x_i} + \frac{u_i u_i}{2}\frac{\partial \rho u_j}{\partial x_j} \tag{64}$$

Note that, since Eq. (58) has been derived by analytically manipulating only temporal derivatives, and since Eq. (64) is the result of substitution of Eqs. (62) and (63) into Eq. (58), it is still valid for the semidiscretized equations. Any further development of Eq. (64) avoiding manipulations, which are not valid for spatially discretized operators (i.e., the product rule), leads to equations, which are still valid at a semidiscrete level.

Upon integration over the domain, one eventually has

$$\frac{d\mathcal{K}}{dt} = -\frac{1}{2}\int_\Omega \left(u_i \frac{\partial \rho u_j u_i}{\partial x_j} + u_i u_i \frac{\partial \rho u_j}{\partial x_j} + \rho u_i u_j \frac{\partial u_i}{\partial x_j} - u_i u_i \frac{\partial \rho u_j}{\partial x_j}\right) d\Omega - \int_\Omega u_i \frac{\partial p}{\partial x_i}\, d\Omega \tag{65}$$

where $\mathcal{K}$ is the integral of ρk over Ω. The first integral in the right-hand side of Eq. (65) is the contribution of the discretization of the nonlinear term to the global kinetic energy equation. This integral is readily seen to be zero, since the second and fourth terms inside the parentheses cancel locally, while the sum of the first and third terms integrated over the domain vanishes by virtue of integration by parts.

By following the same procedure for the Blaisdell form Eq. (61), and applying the splitting to both continuity and momentum equations, one obtains the following nonlinear convective term in the semidiscrete evolution equation for global kinetic energy:

$$-\frac{1}{2}\int_\Omega \left(u_i \frac{\partial \rho u_j u_i}{\partial x_j} + u_i u_j \frac{\partial \rho u_i}{\partial x_j} - \frac{u_i u_i}{2}\left(\frac{\partial \rho u_j}{\partial x_j} - \rho \frac{\partial u_j}{\partial x_j} + u_j \frac{\partial \rho}{\partial x_j}\right)\right) d\Omega \tag{66}$$

which cannot be further simplified upon application of the integration-by-parts rule. This shows that the Blaisdell splitting in not energy preserving.

The Feiereisen skew-symmetric form is not the only splitting that is able to preserve discrete global kinetic energy. Kennedy and Gruber [27] studied a family of splitting forms in which a convex linear combination of all the forms in Eqs. (51)–(55) is used. Although the focus of their paper was to devise a suitable set of coefficients, which is able to minimize aliasing error, their framework is also useful to derive new splittings, which preserve kinetic energy. As observed by Pirozzoli [28], the splitting obtained by weighting the forms $\mathcal{C}^D, \mathcal{C}^\varphi, \mathcal{C}^u$, and $\mathcal{C}^\rho$ with a uniform weight equal to 1/4 is able to preserve kinetic energy, when applied both to momentum and continuity equations (in this last case the form reduces to the symmetric weighting of divergence and advective forms with weight equal to 1/2). This splitting will be hereinafter denoted by Kennedy–Gruber–Pirozzoli (KGP). As for the Feiereisen form, the KGP form is exactly energy preserving provided that central schemes are employed for derivatives, for which the discrete analog of integration by parts holds. A crucial additional point is that both the continuity and the φ-equation have to be discretized with the same form, in order to reproduce the correct balance of the volume average of $\rho\varphi^2$.

More recently, a systematic study of energy preserving forms, among the general family of splittings studied by Kennedy and Gruber [27], has been reported in Ref. [29]. This study has allowed to show that the two above-mentioned forms are actually members of a general two-parameter family of energy-preserving formulations. A simple exemplary result of the theory is the family of forms given by the convex linear combination of Feiereisen $\mathcal{C}^F = (\mathcal{C}^D + \mathcal{C}^\varphi)/2$ and KGP $\mathcal{C}^{\mathrm{KGP}} = (\mathcal{C}^D + \mathcal{C}^\varphi + \mathcal{C}^u + \mathcal{C}^\rho)/4$ forms

$$\mathcal{C}^\alpha = \alpha \mathcal{C}^F + (1-\alpha)\mathcal{C}^{\mathrm{KGP}} \tag{67}$$

Clearly, this one-parameter family provides a consistent expression of the convective nonlinear term and is energy preserving for any value of α. A notable specific case is given by choosing $\alpha = -1$, for which the new simple form is obtained

$$\mathcal{C}^C = \frac{1}{2}\left(\rho\varphi \frac{\partial u_j}{\partial x_j} + u_j \frac{\partial \rho\varphi}{\partial x_j} + \rho \frac{\partial u_j \varphi}{\partial x_j} + \varphi u_j \frac{\partial \rho}{\partial x_j}\right) \tag{68}$$

The new form $\mathcal{C}^C$ is in some sense a symmetric counterpart of $\mathcal{C}^F$, and reduces to the classical advective form when applied to the continuity equation. The family of Eq. (67) can be now expressed in a more symmetric fashion

$$\mathcal{C}^\xi = \xi \mathcal{C}^F + (1-\xi)\mathcal{C}^C \tag{69}$$

with the KGP form corresponding to $\xi = 1/2$. Note that although it is customary to apply the same splitting to continuity and momentum equations, there is no reason to retain this constraint. It can be shown [29] that by relaxing this requirement, more skew-symmetric splittings can be obtained and that the family of Eq. (69) is a restriction of a more general two-parameter family of energy-preserving forms, whose properties are studied in detail therein.

An important topic related to energy-preserving discretizations is that of conservation of linear invariants. A major achievement of the paper by Pirozzoli [28] is that when central explicit finite difference formulas of arbitrary order are used to discretize the

Table 1 Conservation properties induced by different energy balance equation discretized through an energy preserving and locally conservative split form. ⊙: variable conserved locally and globally, ◯: variable conserved globally but not locally, ×: variable not conserved.

		Conserved variable								
		ρ	ρu_i	ρE	ρe	ρs	ρu_i^2	ρE^2	ρe^2	ρs^2
Discretized energy equation	ρE	⊙	⊙	⊙	◯	×	◯	◯	×	×
	ρe	⊙	⊙	◯	⊙	×	◯	×	◯	×
	ρs	⊙	⊙	×	×	⊙	◯	×	×	◯

derivatives, both the Feieresen and the KGP forms can be recast in a locally conservative formulation, i.e., as the difference of numerical fluxes at successive intermediate nodes. Beyond the implications on the convergence to weak solutions, in the presence of shock waves, and on the non-negligible improvement in computational efficiency, this result implies that discrete local and global conservation of linear invariants is guaranteed when the forms $\mathcal{C}^F$ or $\mathcal{C}^{\mathrm{KGP}}$ are employed. This property trivially extends to the whole family $\mathcal{C}^\xi$, which hence constitutes a locally conservative and energy-preserving one-parameter family of forms, when applied simultaneously to the continuity and the φ-equations.

The same considerations made for kinetic energy balance can be equally applied also to the total or internal energy equations. In these cases, a properly constructed "energy-preserving" splitting produces a discretization, which ensures that convective terms do not contribute to the rate of variation of global quantities as ρE^2 or ρe^2, integrated over the domain. Although these quantities have a less prominent physical significance than kinetic energy, experience shows that the fulfillment of these additional requirements typically confers more robustness to the simulations. A variety of approaches can be found in literature. Blaisdell et al. [14] applied their splitting to the internal energy equation, while Feiereisen et al. [26] used the evolution equation for the pressure. Kennedy and Gruber [27] and Pirozzoli [28] used the total energy, although the former split the convective and the pressure terms separately, while Pirozzoli [28] applied the splitting directly to the enthalpy $E + p/\rho$. Honein and Moin [30] applied the Feiereisen splitting to continuity, momentum and entropy equations, and reported great advantages in terms of robustness, supposedly due to preservation of two moments of the entropy (ρs and ρs^2).

A study of the conservation properties of the various approaches is reported in Ref. [29], and the main results are presented in Table 1. The table shows that, by discretizing directly the internal or total energy, the global conservation of entropy is not guaranteed. On the other hand, evolving the entropy equation ensures that ρs is conserved locally and ρs^2 globally, although the conservation of internal or total energy is lost, even in a global sense. Literature results and physical intuition suggest that the fulfillment of as many conservation constraints as possible is desirable and provides additional robustness to the simulation.

2.3.2 Numerical Tests. An illustrative example of the behavior of the various splittings of the convective terms for compressible flow is provided in Fig. 4.

The results show the evolution of total energy for the inviscid Taylor–Green vortex, at $M = 0.1$ (left) and $M = 0.5$ (right), where M is the Mach number. Spatial discretization is achieved by means of a pseudo-spectral method. The domain is a cube of side $2\pi L$, divided into a 32^3 computational mesh. Time integration is performed by a standard RK4 method with fixed time-step, so that the acoustic CFL = 0.5. The splittings of Feiereisen (F), Blaisdell (B), KGP as well as the standard divergence form have been used. The total energy equation is advanced and the same splitting is applied in all equations; in the total energy equation, the splitting is applied to the enthalpy.

The results at the lower Mach number show that only the divergence form is unstable in the time-integration range investigated, with the other forms being able to keep kinetic energy roughly constant (as it should be in light of the quasi-incompressible regime). On the other hand, at $M = 0.5$ the two forms that do not preserve kinetic energy lead to divergence of the computation. The global energy given by the Feiereisen form is also close to diverge, whereas the KGP splitting turns out to be the most robust formulation.

2.4 Additional Topics. The derivations presented in Secs. 2.2 and 2.3 have been purposely carried out using a number of simplifying assumptions, with the aim of illustrating the basic ideas of energy-preserving discretizations. Building upon the ingredients reported in Secs. 2.2 and 2.3, many advanced developments have been accomplished over the years. In the following, some of the most important ones are reviewed in a nonexhaustive fashion.

One topic to preliminarily take into consideration is concerned with the computational cost of energy-preserving methods. In incompressible flows, it was soon recognized that for a regular layout, the skew-symmetric form of convection requires the evaluation of 18 derivatives, whereas only six derivatives are needed for the rotational form; the advective and divergence formulations require nine derivatives [31]. On the other hand, the rotational

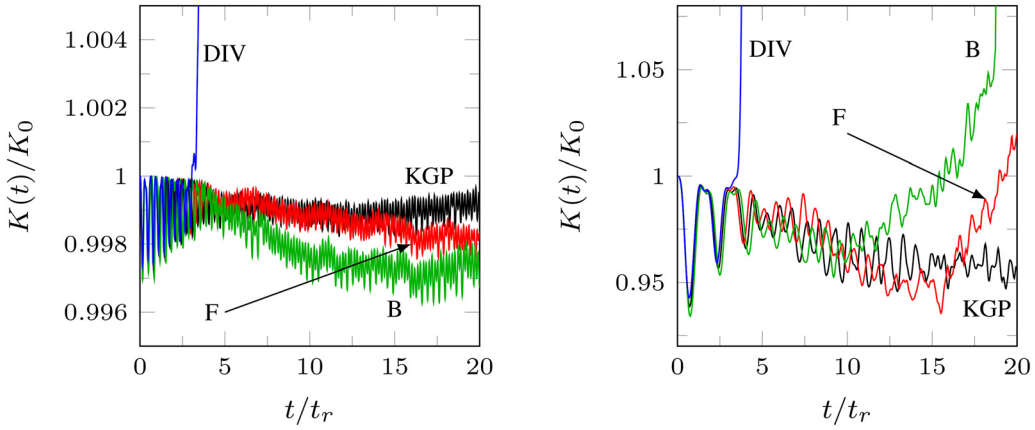

Fig. 4 Comparison of energy-conservation properties of different splittings of the convective terms for the compressible inviscid TGV flow. Left: $M = 0.1$. Right: $M = 0.5$. The splittings refer to the Feiereisen form (F), Eq. (60); the Blaisdell form (B), Eq. (61); the KGP form, obtained by combining Eqs. (51)–(54) with a weight equal to 1/4; the divergence form (DIV), Eq. (51). The reference time is $t_r = L/(Mc)$, where c is the speed of sound.

form does not provide accurate results unless dealiased [15]. The increased cost of the skew-symmetric form is particularly critical for spectral or pseudo-spectral algorithms, in which the pressure Poisson's equation is practically costless and much of the computational time is spent to compute the nonlinear term. Earlier attempts to reduce the cost of the skew-symmetric splitting were merely based on using the divergence and advective forms at alternate time steps [32]. Recently, a more refined approach was proposed by Capuano et al. [22,33–35], in which the divergence and advective forms are instead alternated within the stages of properly designed Runge–Kutta methods. By properly weighting spatial and temporal errors, the authors were able to achieve higher order energy-conservation accuracy while halving the cost for the computation of the convective term. For staggered layouts, the second-order H–W scheme is often the method of choice for turbulent flow simulations, although the additional cost of the interpolation operators is similar to the one occurring for the skew-symmetric form in a regular arrangement. Furthermore, compact derivative approximations [12] able to guarantee local conservation when employed in the divergence form (as in the case of the H–W scheme) have not yet been developed [36], and therefore the use of the skew-symmetric splitting is mandatory for such methods, both on regular and staggered layouts [37,38]. The problem of increased cost comes with even more importance in the case of compressible flows, in which no pressure Poisson equation has to be solved and thus the computation of the nonlinear term constitutes a significant part of the overall solution effort. Pirozzoli [28] analyzed the computational cost of the various forms reported in Sec. 2.3 and reported significant time savings when the splittings were implemented in a locally conservative formulation.

Starting from the basic methods presented in Sec. 2.2.1, many extensions have been proposed in literature over the years, concerning both higher order accuracy and nonregular (i.e., nonuniform, non-Cartesian) meshes. In a landmark paper, Morinishi et al. [9] derived proper fully conservative schemes in regular, staggered, and collocated arrangements. Most notably, they extended the H–W scheme to arbitrary orders of accuracy, although they were not able to retain full conservation (i.e., mass, momentum, kinetic energy) on nonuniform meshes. A further attempt in this direction was later made by Vasilyev [39], who managed to obtain conservation of either momentum or energy, in addition to mass, although not simultaneously if the uniform grid assumption was removed. The first fully conservative scheme on nonuniform Cartesian grids (in both space and time) was proposed by Ham et al. [25], while a fourth-order fully conservative formulation of the H–W method on nonuniform meshes was eventually achieved by Verstappen and Veldman [11]. Remarkably, these authors recognized that the key to obtain kinetic energy conservation at a discrete level on nonuniform grids is to construct the discretization with the aim of preserving the skew-symmetry of the convection operator, rather than minimizing the local truncation error. Using the notation adopted in this work, Eq. (13) is most conveniently rearranged as

$$\mathbf{\Omega}\frac{\mathrm{d}\mathbf{u}}{\mathrm{d}t} + \mathbf{C}(\mathbf{u})\mathbf{u} = -\mathbf{\Omega}\mathbf{G}\mathbf{p} + \frac{1}{\mathrm{Re}}\mathbf{L}\mathbf{u} \tag{70}$$

and the kinetic energy definition generalizes to $\widehat{K} = \mathbf{u}^{\mathrm{T}}\mathbf{\Omega}\mathbf{u}/2$, where $\mathbf{\Omega}$ is a diagonal operator containing the grid spacings. It is readily proven that the condition to preserve kinetic energy in the inviscid limit is again to have a skew-symmetric convective operator $\mathbf{C}(\mathbf{u})$. This is achieved by constructing the discrete differential operators in such a way that this property is satisfied. In other words, the coefficients of the numerical schemes should *not* be weighted with the metrics of the mesh. Although the local truncation error of the resulting symmetry-preserving schemes is not formally as accurate as its counterpart on uniform grids, practical experience has shown that results are reliable, even on coarse meshes [11]. Energy-preserving methods have also been developed for cylindrical coordinates. Starting from the pioneering work by Verzicco and Orlandi [40], which does not strictly conserve energy, subsequent refinements were proposed by Fukagata and Kasagi [41] and Morinishi et al. [42] for incompressible flows. This latter method was then extended to variable-density flows by Desjardins et al. in a formulation that discretely conserves mass, momentum, and kinetic energy in a periodic domain [43].

Further developments of the basic ideas of skew-symmetry in the context of compressible flows were extended to finite volume methods [44] and to curvilinear meshes [45,46]. An alternative approach to the one presented in Sec. 2.3 that has both mathematical and practical significance is the so-called *square-root* variable formulation. In this case, the state vector of the compressible flow solution is expressed as

$$\mathbf{q} = \begin{bmatrix} \sqrt{\rho} \\ \sqrt{\rho}\mathbf{u}/\sqrt{2} \\ \sqrt{\rho e} \end{bmatrix} \tag{71}$$

The square-root formulation has several interesting properties. The global norm of the state vector $||\mathbf{q}||^2$ is bounded in absence of external sources, as it turns out to be the sum of mass and total energy integrated over the domain. Therefore, methods preserving linear invariants (such as finite volume methods) satisfy this property. On the other hand, computations may still break down due to violation of other conservation properties by the convective terms. In this regard, it is interesting to observe that all the quantities preserved by convection (e.g., mass, momentum, kinetic energy, internal energy) can be expressed as quadratic forms of the square-root variables, $q_i q_j$. It has been shown that this is a direct consequence of the skew-symmetry of the convective transport for the square-root variables, in full analogy with the incompressible case [47]. Building upon this mathematical framework, symmetry-preserving methods for compressible flows have been recently proposed [48,49]. A rigorous treatment of skew-symmetry in variable-density flows has also been developed by Morinishi [50].

Discrete conservation principles have also been extended in the context of unstructured meshes. Perot [51] developed a staggered mesh method on two-dimensional unstructured grids able to preserve either kinetic energy and momentum (using the divergence form of convection) or kinetic energy and vorticity (using the rotational form). The method was then extended to three-dimensional grids by Zhang et al. [52]. Later, Mahesh et al. [18] proposed an energy-conserving algorithm, which uses the rotational form in a staggered layout and is fully conservative for tetrahedral elements. For elements of more general shape, they switched to a nonstaggered formulation which is not fully conservative due to the spurious contribution of the pressure gradient. This latter issue has been thoroughly analyzed by Felten and Lund [10]. Recently, based on the work by Verstappen and Veldman, a fully conservative method on unstructured meshes has been presented on a collocated layout, with special emphasis on preventing the pressure odd-even decoupling [53]. Again, the key ingredients leading to a skew-symmetric convective operator were identified in (1) interpolating the transported variable with *constant* weights (i.e., independent of the spatial coordinates), and (2) a properly defined divergence operator ensuring that the sum of the discrete velocity fluxes at the cell faces sums to zero for each computational cell. In the context of compressible flow, Modesti and Pirozzoli [54] have proposed an unstructured implementation of the KGP split form (cf. Sec. 2.3) and also used it as a building block to solve flows with shocks.

A further topic of remarkable interest is the enforcement of boundary conditions such that the skew-symmetry of the difference operators is retained. The basic idea is to ensure that the global discrete differential operators, after inclusion of the boundary conditions, still possess a discrete *summation-by-parts* rule.

For dedicated reviews on summation-by-parts schemes, the reader is referred to Refs. [55] and [56]. Recently, boundary conditions that satisfy secondary conservation properties were derived by Sanderse et al. [57] with particular reference to the fourth-order extensions of the H–W method mentioned previously.

In addition to kinetic energy, which is the primary focus of this work, additional quadratic invariants can be in principle considered. The reader is referred to the paper by Olver [58] for a comprehensive and elegant derivation of the inviscid invariants of the incompressible Navier–Stokes equations based on the Hamiltonian formalism. Most notably, the inviscid flow equations also preserve the total enstrophy $\int_\Omega \boldsymbol{\omega}\cdot\boldsymbol{\omega}\,\mathrm{d}\Omega$ and the total helicity $\int_\Omega \mathbf{u}\cdot\boldsymbol{\omega}\,\mathrm{d}\Omega$ of the flow in two and three dimensions, respectively, with $\boldsymbol{\omega}=\nabla\times\mathbf{u}$ being the vorticity field. These quadratic quantities have important theoretical and practical significance [59], and therefore it is appealing to derive numerical methods able to preserve them at a discrete level. For two-dimensional flows, discrete conservation of enstrophy has received considerable attention especially in the context of finite- and spectral-element methods [60,61]. In contrast, invariance of helicity has been rarely considered, with notable exceptions including the works by Liu and Wang [62], for axisymmetric flows, and by Rebholz and coworkers (see, e.g., Refs. [63–65]), in the framework of finite element methods. Recently, the effects of discrete energy and helicity conservation for helical flows have been discussed by Capuano and Vallefuoco [66].

Current research trends tend to apply the concepts of energy conservation in situations of constantly increasing complexity. The viability of DNS and LES for flows of engineering interest has increased the demand for robust and efficient numerical discretizations, and therefore the concepts of discrete conservation principles are being analyzed in physical models which are progressively more sophisticated. For instance, recent works deal with energy-preserving methods for multiphase flows [67], as well as with moving meshes [68]. Furthermore, the present review has focused on finite difference and finite volume methods, in which energy-conserving methods have historically originated. However, in recent years, the concepts discussed in this work have started to be transferred also to other discretization techniques, such as finite element and discontinuous Galerkin (DG) methods, which are being increasingly used for turbulent flow simulations especially in the context of complex engineering applications. In this regard, we mention the recent work by Charnyi et al. [69] (references therein are also worth consulting), who proposed a finite element discretization of the incompressible Navier–Stokes equations that conserves energy, momentum, as well as other important quantities. This method has been recently applied in conjunction with pseudo-symplectic Runge–Kutta schemes (that will be presented in Sec. 3) for the simulation of vortex-induced vibrations of a circular cylinder [70]. Discontinuous Galerkin methods are often employed in under-resolved computations of turbulence for implicit large-eddy simulation purposes [71]. Therefore, an accurate control of aliasing errors and nonlinear stability is of fundamental importance. Recently, split forms for compressible flow that preserve kinetic energy have been developed for DG schemes [72,73], and compared to dealiasing techniques [74].

A number of "industrial" applications of some of the methods discussed in this section are presented in Sec. 4.

3 Temporal Conservation

In this section, the energy-conservation properties of the time integrator are analyzed. Temporal conservation errors generally arise for both incompressible and compressible flow simulations; in the following, we will focus particularly on the incompressible case, and briefly mention the compressible one at the end of the section.

Once the incompressible N–S equations have been spatially discretized, one is left with Eqs. (13) and (14), for which a further discretization in time is required. Due to the continuity equation, which is a kinematic constraint on the velocity field ensuring that the incompressibility condition is satisfied at each time-step, semi-discretization yields an index-2 differential algebraic system [8]. By introducing a projection operator $\mathbf{P}$, it can be formally recast as a system of ODE

$$\frac{\mathrm{d}\mathbf{u}}{\mathrm{d}t}=\widetilde{\mathbf{F}}(\mathbf{u})\mathbf{u} \tag{72}$$

where $\widetilde{\mathbf{F}}=\mathbf{PF}$ and $\mathbf{F}(\mathbf{u})=-\mathbf{C}(\mathbf{u})+(1/\mathrm{Re})\mathbf{L}$, with $\mathbf{P}=\mathbf{I}-\mathbf{G}\mathcal{L}^{-1}\mathbf{M}$ and $\mathcal{L}=\mathbf{MG}$. Time advancement of Eq. (72) is now straightforward and can be carried out by means of any ODE solver. Note that the role of the projection operator is to enforce incompressibility at each time instant through the solution of a Poisson's equation for pressure [75]. In the inviscid limit, the system of ODE is left at the right-hand side with the term $\widetilde{\mathbf{C}}(\mathbf{u})=\mathbf{PC}(\mathbf{u})$. When a global energy-conserving spatial discretization is employed, the matrix $\mathbf{C}$ is skew-symmetric, which in turn implies $\mathbf{u}^{\mathrm{T}}\widetilde{\mathbf{C}}\mathbf{u}=0$ for all $\mathbf{u}$ satisfying $\mathbf{Mu}=0$. Under such hypotheses, Eq. (72) is an ODE system possessing kinetic energy as a quadratic invariant. Similarly to the case of spatial discretization, general-purpose time-advancement methods do not necessarily ensure preservation of invariants at the (time-) discrete level. More specifically, while all Runge–Kutta (RK) and linear multistep methods preserve linear invariants [76], preservation in time of quadratic invariants is possible only for some special implicit RK methods [77,78]. We will thus restrict ourselves to the class of RK time-advancement methods.

Since the pioneering works from the Stanford group [79], RK methods have become very popular in the fluid dynamics community due to their favorable properties, such as their self-starting capability and relatively large stability limit. The majority of turbulence simulations are nowadays performed by using three-stage (particularly the low-storage Wray's scheme [80]) or four-stage (the classical RK4 [81]) methods in conjunction with fractional-step procedures. For wall-bounded flows, the viscous term is sometimes treated implicitly (e.g., using a Crank–Nicolson scheme) to overcome the stability restriction of explicit schemes [82].

A general s–stage RK method applied to Eq. (72) can be expressed as

$$\mathbf{u}^{n+1}=\mathbf{u}^{n}+\Delta t\sum_{i=1}^{s}b_i\widetilde{\mathbf{F}}(\mathbf{u}_i)\mathbf{u}_i \tag{73}$$

$$\mathbf{u}_i=\mathbf{u}^{n}+\Delta t\sum_{j=1}^{s}a_{ij}\widetilde{\mathbf{F}}(\mathbf{u}_j)\mathbf{u}_j \tag{74}$$

where a_{ij} and b_i are the RK coefficients. The RK coefficients are often arranged into the so-called Butcher tableau [83], and are usually constructed to maximize the temporal order of accuracy of the method, hereinafter referred to as *classical* order p (or simply order).

The energy-conservation properties of an RK method can be analyzed by deriving an expression for the kinetic energy variation introduced by Eqs. (73) and (74). The fully discrete evolution equation can be obtained in closed form by taking the inner product between $\mathbf{u}^{n+1}$ and itself. After some basic manipulations, one has

$$\frac{\Delta\widehat{K}}{\Delta t}=\frac{1}{\mathrm{Re}}\sum_{i}b_i\mathbf{u}_i^{\mathrm{T}}\mathbf{L}\mathbf{u}_i-\frac{\Delta t}{2}\sum_{i,j=1}^{s}(b_ia_{ij}+b_ja_{ji}-b_ib_j)\mathbf{u}_i^{\mathrm{T}}\widetilde{\mathbf{F}}_i^{\mathrm{T}}\widetilde{\mathbf{F}}_j\mathbf{u}_j \tag{75}$$

where $\Delta\widehat{K}=\widehat{K}^{n+1}-\widehat{K}^{n}$ and $\widetilde{\mathbf{F}}_i=\widetilde{\mathbf{F}}_i(\mathbf{u}_i)$. Note that Eq. (75) in various different forms has been derived in Refs. [22], [84], and [85], among others. Equation (75) is the fully discrete counterpart of the continuous kinetic energy equation, Eq. (12), which can be rearranged as

$$\frac{\Delta K}{\Delta t} = -\frac{1}{\mathrm{Re}}\frac{1}{\Delta t}\int_t^{t+\Delta t} \phi \mathrm{d}t \tag{76}$$

where $\phi = \int_\Omega 2S_{ij}S_{ij}\,\mathrm{d}V$ is the scalar dissipation function. Note that the quantity $\mathbf{u}_i^T\mathbf{L}\mathbf{u}_i$ is the spatially discretized version of ϕ. Equation (75) differs from Eq. (76) due to the presence of the second term on the right-hand side, which represents the temporal error. It is worth noting that the appearance of an additional term in Eq. (75) can be interpreted as a consequence of the lack of the discrete summation-by-parts rule from the RK discrete time operator [66].

Energy-conserving RK methods possess the following property:

$$M_{ij} = b_i a_{ij} + b_j a_{ji} - b_i b_j = 0 \qquad \forall\, i,j = 1,\ldots,s\,. \tag{77}$$

The fulfillment of the above conditions allows to preserve the global kinetic energy (for inviscid flows), or to enforce the correct discrete kinetic energy balance (for viscous flows). In other words, it ensures that the variation of kinetic energy is solely due to the physical viscous dissipation. The condition on the coefficients in Eq. (77) is popular in the ODE community and is commonly referred to as the *M-condition*; it can only be satisfied by implicit methods. The fulfillment of the M-condition can be shown to provide conservation of all quadratic invariants, thus including kinetic energy for the inviscid N–S equations. Furthermore, for irreducible RK methods, Eq. (77) is also a necessary and sufficient condition for *symplecticity* [78]. Indeed, RK methods that satisfy $M_{ij} = 0$ are also known as *symplectic*, and are the methods of choice for conservative (Hamiltonian) problems. Some examples of standard and symplectic RK schemes are reported in Table 2.

Energy-conserving time-integration methods have been applied only a few times in the context of incompressible flow equations. Ham et al. [25] developed a fully conservative algorithm based on the midpoint method, which proved to preserve energy in time exactly in inviscid computations. Verstappen and Veldman [11] also applied the implicit midpoint rule to their symmetry-preserving spatial discretization and recognized that the resulting scheme is unconditionally stable on any mesh size and for any time-step. More recently, Sanderse [85] carried out a systematic study of symplectic methods, including higher order ones, for the incompressible N–S equations. The relationship between energy conservation and time reversibility was also discussed, showing that there exist methods, which are energy conserving but not time reversible, and vice versa. This should be carefully taken into consideration, especially when using time reversibility as a benchmark for energy conservation, as suggested in Ref. [86]. Symplectic methods were generally found to give good results, although a complex nonlinear system has to be solved to advance in a single time-step, leading to implementation issues and remarkable computational effort, especially for the higher order ones (e.g., the Radau method given in Table 2).

Despite the favorable properties of symplectic methods, explicit schemes are usually preferred for turbulence simulations, especially when the time-step size is dictated by accuracy and not by the stability constraint [87]. Furthermore, explicit schemes are more suited to massively parallel computing, which is now a mandatory requirement for DNS and LES of turbulence.

For explicit schemes, the Butcher tableau is lower triangular, i.e., $a_{ij} = 0$ for $j \geq i$. In this case, the temporal error in Eq. (75) cannot be nullified. Instead, for $\mathrm{Re} \to \infty$, one has

$$\frac{\mathrm{d}\widehat{K}}{\mathrm{d}t} = \mathcal{O}(\Delta t^q) \tag{78}$$

where q is the *pseudo-symplectic order*. In standard methods, one usually has $p = q = s$. However, special methods can be constructed in which the coefficients are derived to satisfy additional conditions such that the error term in Eq. (75) is of order $q > p$. These pseudo-symplectic order conditions have been obtained by Aubry and Chartier [88] by employing the theory of trees; they are reported in Table 2.1 of the same work up to sixth-order. The order conditions can be equivalently obtained by expanding Eq. (75) as a Taylor series in the time increment Δt. By using the linearity of the convective operator $\mathbf{C}(\mathbf{u}_i)$ and substituting Eqs. (73) and (74) into Eq. (75), one obtains

$$\begin{aligned}\frac{\Delta K}{\Delta t} = &-\Delta t\left[C_2\sum_{ij} M_{ij}\right] - \Delta t^2\left[C_3\sum_{ijk} M_{ij}a_{jk}\right]\\ &-\Delta t^3\left[C_{4,1}\sum_{ijkl} M_{ij}a_{ik}a_{kl} + C_{4,2}\sum_{ijkl} M_{ij}a_{ik}a_{jl}\right]\\ &-\Delta t^4\left[C_{5,1}\sum_{ijklm} M_{ij}a_{ik}a_{jl}a_{jm} + C_{5,2}\sum_{ijklm} M_{ij}a_{jk}a_{kl}a_{im}\right.\\ &+C_{5,3}\sum_{ijklm} M_{ij}a_{jk}a_{kl}a_{jm} + C_{5,4}\sum_{ijklm} M_{ij}a_{jk}a_{kl}a_{km}\\ &\left.+C_{5,5}\sum_{ijklm} M_{ij}a_{jk}a_{kl}a_{im}\right] + \mathcal{O}(\Delta t^5)\end{aligned} \tag{79}$$

The various coefficients C are scalar functions that can be expressed as combinations of the convective operator. For further details about the derivation of Eq. (79), the reader is referred to Refs. [22] and [33]. The pseudo-symplectic order conditions can be easily obtained by nullifying the single independent terms in Eq. (79), and can be shown to be equivalent to those presented

Table 2 Examples of standard (Wray's RK3 and RK4) and symplectic RK schemes. Note that the Wray's scheme has been recast in standard (no low-storage) form.

Wray's RK3

	0		
$\frac{8}{15}$	$\frac{8}{15}$	0	
$\frac{2}{3}$	$\frac{1}{4}$	$\frac{5}{12}$	0
	$\frac{1}{4}$	0	$\frac{3}{4}$

RK4

	0			
$\frac{1}{2}$	$\frac{1}{2}$	0		
$\frac{1}{2}$	0	$\frac{1}{2}$	0	
1	0	0	1	0
	$\frac{1}{6}$	$\frac{1}{3}$	$\frac{1}{3}$	$\frac{1}{6}$

Gauss

$\frac{1}{2}$	$\frac{1}{2}$	
	1	

Radau IIB

$\frac{1}{3}$	$\frac{3}{8}$	$-\frac{1}{24}$
1	$\frac{7}{8}$	$-\frac{1}{8}$
	$\frac{3}{4}$	$\frac{1}{4}$

Table 3 Examples of pseudo-symplectic methods (from Refs. [88] and [89]). The notation indicates the order on solution *p* and on energy conservation *q*; the number in brackets is the number of stages *s*.

3p5q(4)	3p6q(5)	4p7q(6)
$a_{21}=3/8$	$a_{21}=0.13502027922909$	$a_{21}=0.23593376536652$
$a_{31}=11/12$	$a_{31}=-0.47268213605237$	$a_{31}=0.34750735658424$
$a_{32}=-2/3$	$a_{32}=1.05980250415419$	$a_{32}=-0.13561935398346$
$a_{41}=-1/12$	$a_{41}=-1.21650460595689$	$a_{41}=-0.20592852403227$
$a_{42}=11/6$	$a_{42}=2.16217630216753$	$a_{42}=1.89179076622108$
$a_{43}=-3/4$	$a_{43}=-0.37234592426536$	$a_{43}=-0.89775024478958$
$b_1=1/9$	$a_{51}=0.33274443036387$	$a_{51}=-0.09435493281455$
$b_2=8/9$	$a_{52}=-0.20882668296587$	$a_{52}=1.75617141223762$
$b_3=-2/9$	$a_{53}=1.87865617737921$	$a_{53}=-0.96707850476948$
$b_4=2/9$	$a_{54}=-1.00257392477721$	$a_{54}=0.06932825997989$
	$b_1=0.04113894457092$	$a_{61}=0.14157883255197$
	$b_2=0.26732123194414$	$a_{62}=-1.17039696277833$
	$b_3=0.86700906289955$	$a_{63}=1.30579112376331$
	$b_4=-0.30547139552036$	$a_{64}=-2.20354136855289$
	$b_5=0.13000215610576$	$a_{65}=2.92656837501595$
		$b_1=b_6=0.07078941627598$
		$b_2=b_5=0.87808570611881$
		$b_3=b_4=-0.44887512239479$

in Ref. [88]. By properly coupling the classical and pseudo-symplectic order conditions, *pseudo-symplectic* RK methods with prescribed orders of accuracy p and q can be derived [89,90]. Examples of such methods are reported in Table 3.

A comparison of standard, symplectic, and pseudo-symplectic methods in terms of energy-conservation properties is illustrated by two basic examples. Figure 5 (left) shows the time evolution of the global energy error

$$\sigma_K(t)=\frac{\widehat{K}(t)-\widehat{K}_0}{\widehat{K}_0} \tag{80}$$

for an inviscid double mixing layer flow (see Ref. [22] for further details). Spatial discretization is accomplished on a 40^2-cells mesh by means of the second-order H–W energy-conserving method mentioned earlier. The final time is $t=8$, at which the shear layer roll-up is well defined and the mixing layer instability has fully entered its nonlinear phase. All cases have been integrated with a fixed time-step corresponding to CFL = 1.0. In this case, global energy is solely changed by the temporal dissipation, see Eq. (75). The error magnitudes of the pseudo-symplectic schemes are much lower with respect to the Wray's and RK4 methods. On equal number of stages, the 3p5q method provides superior energy-conservation properties with respect to the RK4, especially during the early evolution; at later times, the two schemes provide similar results. The best results are achieved with the 3p6q and 4p7q schemes, which nevertheless require one and two additional stages, respectively, as compared to the RK4. The symplectic Gauss's method provides a null (to machine accuracy) energy-conservation error.

A more complex test is the canonical three-dimensional Taylor-Green vortex described earlier. In this case, the global energy balance is modified by both the (physical) scalar dissipation rate and the temporal error, and Eq. (75) can be conveniently rearranged as

$$\frac{\Delta\widehat{K}}{\Delta t}=\frac{1}{\mathrm{Re}}\overline{\Phi}+\varepsilon^{\mathrm{RK}}\equiv\varepsilon^{\nu}+\varepsilon^{\mathrm{RK}}\equiv\frac{1}{\mathrm{Re}_{\mathrm{eff}}}\overline{\Phi} \tag{81}$$

where the *effective Reynolds number* $\mathrm{Re}_{\mathrm{eff}}$ has been defined. The time evolution of the ratio between the molecular dissipation to the temporal error rates is reported in Fig. 5 (right) for two nominal Reynolds numbers, Re = 1600 and Re = 3000. Simulations are carried out in this case by means of a fourth-order Padè scheme [12] in skew-symmetric form on a 64^3 mesh. All computations are again performed with a fixed time-step corresponding to CFL = 1.0. The plot shows that standard RK3 and RK4 methods commonly used in the turbulence community can lead to a significant amount of dissipation, which clearly increases as the flow becomes more under-resolved. Particularly, at the moment of transition to turbulence, the RK3 scheme provides an effective Reynolds number that is about 15% less than the nominal one, thus remarkably violating the physical significance and reliability of the simulation. On the other hand, the pseudo-symplectic methods give negligible dissipation values. Again, the symplectic Gauss method provides a temporal dissipation, which is null to machine accuracy. For this test, the implicit scheme was about 2.5 times slower than the RK4, using a fixed-point iteration method with a tolerance equal to 10^{-14}. The implicit solver needed on average 8 iterations per time-step to converge.

Clearly, the numerical dissipation of a time-integration scheme can be decreased by reducing the time-step size; a recent numerical study has shown that pseudo-symplectic methods are globally more efficient than standard ones, being able to provide the same dissipation levels with a reduced number of time steps [91]; in the same study, the interaction of the temporal errors with subgrid-scale models is also discussed. Further work is underway to derive an adaptive time-stepping strategy relying on an error controller based on the temporal dissipation [92]. Note that Eq. (81) can be either interpreted as an *instantaneous* balance, i.e., the energy variation occurring between two consecutive time steps, or alternatively as a *cumulative* budget, namely the variation between the global energy at a certain time with respect to the initial energy.

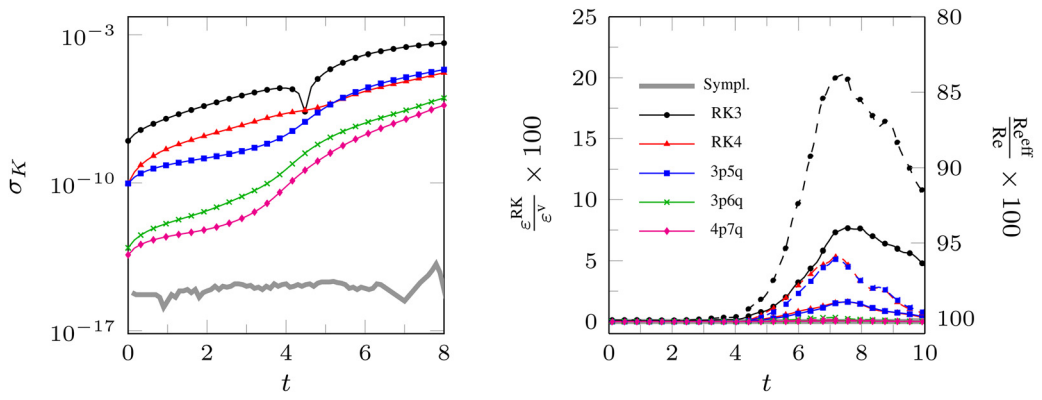

Fig. 5 Comparison of energy-conservation properties of different temporal schemes. Left: energy-conservation error for the 2D inviscid double mixing layer. Right: ratio of temporal to physical dissipation rates for a 3D TGV at Re = 1600 (solid lines) and Re = 3000 (dashed lines) for various standard, symplectic and pseudo-symplectic RK methods.

In this latter case, the physical and numerical viscosities should be accumulated in time, leading to the plot reported in Fig. 2 of Ref. [89].

In the context of compressible flows, temporal conservation errors are more difficult to characterize when using conservative variables. Indeed, in this usual setting, quadratic quantities that are preserved by convection cannot be expressed as pure products of the evolved variables. Compressible flow simulations typically employ explicit RK methods with strong-stability preserving or low-dispersion properties for accurate aeroacoustic computations [93–95]. Apparently, there have been no studies to date to characterize conservation errors due to temporal integration in this framework. However, it has been recently observed that, when using the square-root formulation mentioned in Sec. 2.4, all the relevant conserved quantities are quadratic products of the type $q_i q_j$ of the state vector $\mathbf{q}$ [48,49]. Therefore, their fully discrete evolution is characterized by an equation similar to Eq. (75), and all the properties of symplectic methods mentioned for the incompressible flow also apply for the compressible case. Most likely, this holds true also for the pseudo-symplectic schemes. This finding generalizes to arbitrary order the second-order conservative methods previously proposed by Subbareddy and Candler [96] and Morinishi [50].

4 Applications

Since the early developments, energy-preserving numerical methods have been typically employed in academic solvers, often in conjunction with high-order numerical schemes both in space and time [79,97]. On the other hand, stability and robustness in complex geometries and configurations of engineering interest have been traditionally accomplished by low-order central-differencing schemes with either local upwinding [98,99] or explicit filtering [100,101], at some expense of solution fidelity. Indeed, the introduction of artificial dissipation, in any form, to the numerical algorithm is known to be detrimental to the quality and reliability of the solution, especially for large-eddy simulation of turbulence [102,103]. The application of energy-conserving methods to industrial CFD is relatively recent and can be dated back to the early 2000s, when discrete conservation principles started to be extended to curvilinear or unstructured meshes, as already outlined in Sec. 2.4. Since then, energy-conserving algorithms have been employed for DNS and LES of turbulent flows in several areas of applied science, e.g., aerodynamics, combustion, high-pressure mixing, as well as many others. Numerous examples can be found in literature, spanning several fields of application as well as a broad range of flow regimes and computational complexity. Far from being exhaustive, this section aims to review some recent examples, with particular reference to cases in which enforcement of energy conservation provided significant advantages over standard methods, in terms of robustness and reliability of the results.

External aerodynamics has largely benefited from the development of energy-conserving methods. Some early attempts, particularly with reference to large-eddy simulation of flow over airfoils on curvilinear/unstructured meshes, were summarized in the context of the LESFOIL project [105]. Some of the simulations displayed severe unphysical wiggles when using straightforward central-differencing schemes, and the noise could only be removed by adding numerical dissipation in certain regions of the flow. Subsequently, these results were re-interpreted in terms of energy-conservation properties by You et al. [104], who performed incompressible large-eddy simulations of flow over an airfoil with separation control. The authors compared central-differencing solvers with and without enforcement of discrete energy conservation; results are shown in Fig. 6. The energy-preserving algorithm, based on the scheme developed by Mahesh et al. [18] (cf. Sec. 2.4), was able to suppress the wiggles without introducing any artificial dissipation to the flow, thus highly enhancing the fidelity of the results.

Energy-preserving methods have also been used for transonic aerodynamics. Recently, Modesti and Pirozzoli [54] performed inviscid computations of the ONERA M6 wing [106] using an unstructured compressible flow solver relying on the KGP split formulation for the convective term (cf. Sec. 2.3), with shock-capturing capabilities provided by a classical AUSM splitting scheme [107] with a shock sensor [108]. Their solver, named *rhoEnergyFoam*, was implemented into the open-source library OPENFOAM [109] and compared to the native OPENFOAM compressible solver *rhoCentralFoam*, that employs the total-variation diminishing (TVD) scheme by Kurganov and Tadmor [110]. Sample results are reported in Fig. 7 (courtesy of D. Modesti and S. Pirozzoli). Important qualitative and quantitative differences emerge from the comparison of the two numerical solutions: overall, the dissipative solver *rhoCentralFoam* provided smeared shocks (especially at the leading edge) due to its inherent numerical diffusion. On the other hand, the energy-preserving solver was able to correctly predict the strength and position of the shocks and provided very good agreement with experimental data.

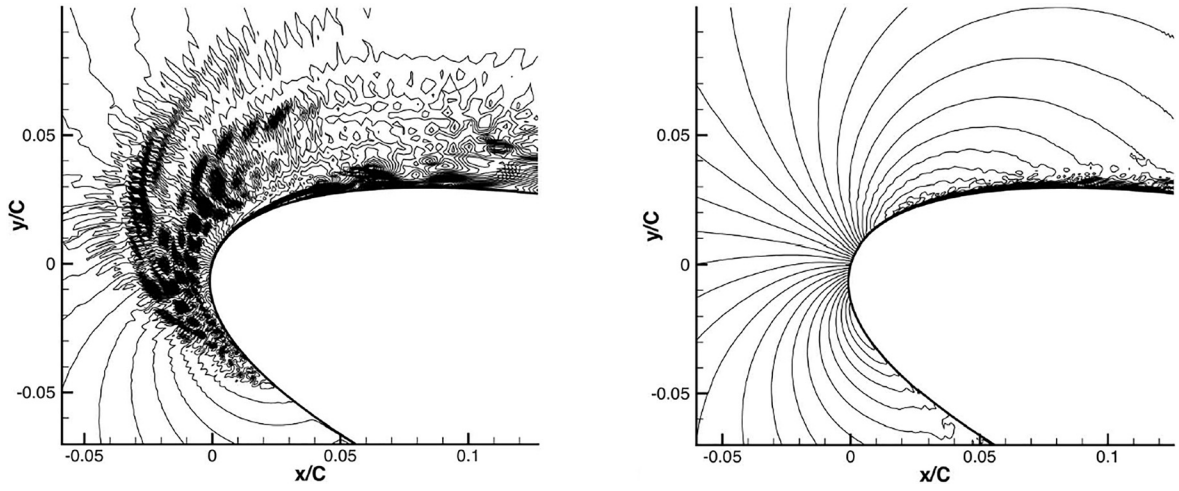

Fig. 6 Contour plots of the instantaneous streamwise velocity component u/U_∞ predicted by LES based on a non-dissipative scheme without discrete kinetic energy conservation (left) and with a solver that preserves kinetic energy (right). Shown are 30 levels in the ranges of −0.43 to 2.58). Reproduced from Ref. [104] with permission from AIP Publishing.

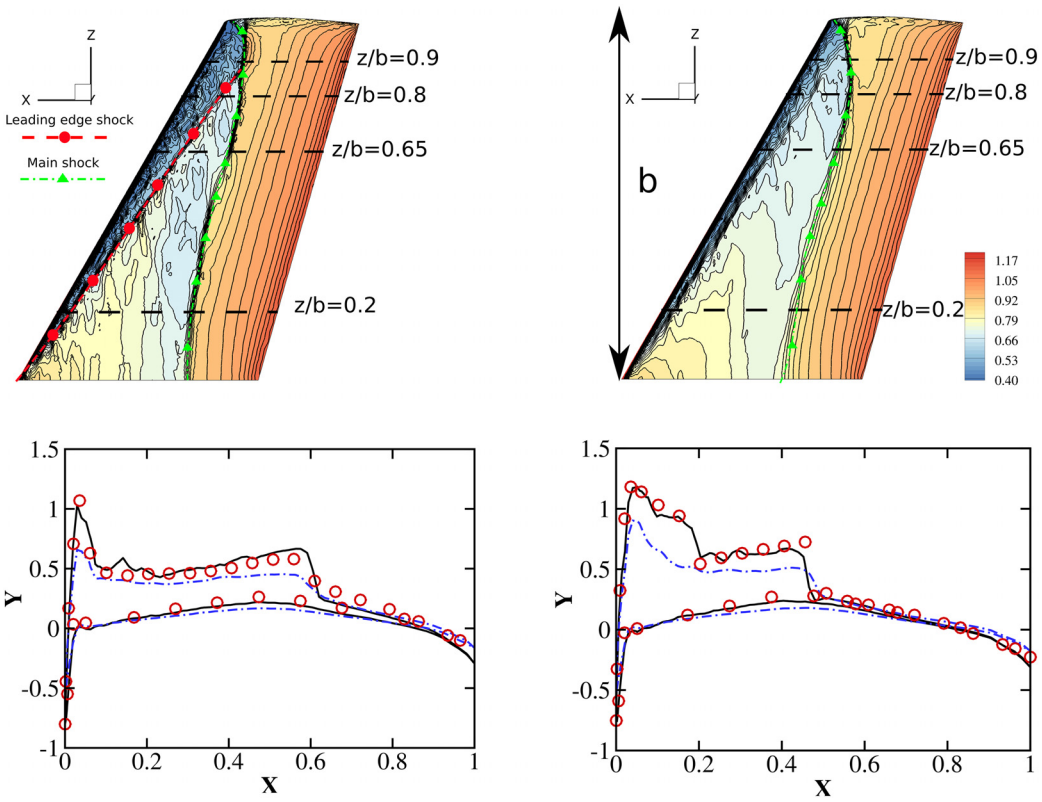

Fig. 7 Results for the flow around ONERA M6 wing. Top: pressure contours on the wing surface for *rhoEnergyFoam* (left) and *rhoCentralFoam* (right); shown are 32 levels in the range $0.4 \le p/p_\infty \le 1.2$. Bottom: spatial distribution of the pressure coefficient along the chord at sections $z/b = 0.2$ (left) and $z/b = 0.65$ (right) for *rhoEnergyFoam* (solid lines) and *rhoCentralFoam* (dot-dashed lines), compared to experimental data (circles). Figure courtesy of D. Modesti and S. Pirozzoli.

Several additional examples of successful application of energy-preserving schemes to external aerodynamics can be found in recent years. The group of Oliva and coworkers has applied the symmetry-preserving unstructured method developed by Trias et al. [53] to study complex flows over a car model [111,112], a NACA0012 in full stall [113], and a circular cylinder [114]. Rozema et al. [115] investigated the flow over a delta wing using a fourth-order symmetry-preserving scheme for compressible flow derived in the framework of the square-root formulation [48] (cf. Sec. 2.4) and extended to curvilinear structured meshes.

Energy-conserving solvers have also been widely used in the context of turbulent combustion and high-pressure injection applications. In such problems, capturing of small-scale mixing is essential and benefits coming from discrete conservation principles are emphasized [116]. Simulations of realistic combustion devices were prompted by the development of high-fidelity, fully unstructured CFD codes such as AVBP of the CERFACS group [117], and CDP of the Stanford group. This latter solver, later evolved in Charles, is based on the energy-preserving, unstructured algorithm proposed by Mahesh et al. [18] and later refined by Ham and Iaccarino [118]. These capabilities allowed the *famous* simulation of the Pratt & Whitney, East Hartford, CT gas turbine combustor reported in Ref. [119]. An additional example is the solver SiTCom-B developed at CORIA [120], which implements the fourth-order, skew-symmetric finite volume method proposed by Ducros et al. [44]. The solver has been massively used to investigate combustion and high-pressure mixing [121,122].

As a final remark, it is interesting to observe that the overwhelming majority of multipurpose CFD codes, either open-source or commercial, are currently not provided with energy-conserving schemes. Rather, they rely on numerical diffusion to increase the solver robustness. For instance, to the author's knowledge and practical experience, and also upon inspection of the specialized literature, the native solvers coming with OPENFOAM do not preserve kinetic energy by convection in the inviscid limit, in both their incompressible and compressible implementations. Some researchers have recognized this deficiency and have recently proposed and implemented low-dissipative algorithms [54,123,124].

5 Conclusions

In numerical simulations of the Navier–Stokes equations, energy-preserving methods have received much attention in past years, and are now considered a key element for stable and reliable numerical discretizations, both in direct and large eddy simulations of turbulence. In this paper, a survey of the most successful approaches in this field has been presented. The emphasis has been mainly put on ideas, with careful exposition of techniques in simplified settings. Starting from the illustration of some of the important features of the continuum models, the discussion on numerical approaches has been conducted by separately considering incompressible and compressible flows, and has covered spatial and temporal discretizations.

The analysis has been carried out by first considering the topic of spatial conservation for incompressible flows, since the set of techniques and results in this field constitute the classical cornerstone for energy preserving methods. The theory has been exposed by adopting a matrix notation for the discrete operators, which can be, in our opinion, an efficient tool to justify many properties of the discretization in simple settings. The regular layout has shown to be the simplest and more effective environment in which the main ingredient for energy conservation, i.e., the skew-symmetry of the discrete convective operator, can be recognized. It has been shown that energy conservation can be achieved by means of the so-called skew-symmetric form of the nonlinear

term, which, by construction, assures the skew-symmetry of the discrete convective operator. The employment of the matrix notation in the staggered case, on the other hand, has shown that the additional degrees-of-freedom associated with the interpolation procedure lead to the possibility of obtaining globally skew-symmetric discrete operators also for the divergence form. The reason for this difference lies in the fact that the staggering of the variables, and the associated additional interpolation step, actually permits to enforce a discrete version of the product rule, a crucial element, which is missing in the regular layout.

The compressible case has been analyzed in detail within the classical framework of the "split" forms of the nonlinear terms, which possess a cubic nonlinearity. The exposition of the properties of the classical Feiereisen and Blaisdell forms has been complemented with the analysis of more recent split forms, together with a resume of a general framework that has been recently developed. The topics of conservation of linear invariants and of the choice of which energy equations is more suitable to discretize for stability and reliability are also commented on. Extensions and applications to more complex settings are separately reviewed, with particular attention to recent developments.

Temporal energy conservation, i.e., the property of temporal integration to retain the quadratic invariants of the continuous model, has also been considered. Since the errors arising from RK integration are typically dissipative, temporal energy conservation was considered not harmful for stability, and this topic has received scarce attention in the past. However, as shown in the paper, standard methods can provide a non-negligible amount of dissipation, which can violate the physical reliability of the simulations. The recent theory of pseudo-symplectic RK schemes, with emphasis on the application to N–S equations and to turbulent regimes, has been exposed with full details. Pseudo-symplectic schemes have proven to be effective in reducing the numerical dissipation, and it is expected that the topic of temporal energy conservation will be further explored in the near future.

All the discussed techniques and all the properties of the various approaches have been neatly illustrated by numerical simulations of canonical turbulent flows. In addition, a separate section of industrial or "real-world" applications has been included. The implementation of energy-preserving methods in complex configurations is recent, and most of the commercial codes employed for industrial calculations still employ low-order schemes, which allow the fulfillment of stable simulations by means of some form of artificial dissipation. Among the various applications of the open literature, which are here reviewed, we highlighted some recent studies with the aim of showing the beneficial effects of energy preserving discretizations in real-world and industrial applications.

The main challenge of near future research is probably an efficient and accurate extension of some of the many concepts here illustrated to complex multiphysics configurations and to unstructured meshes. Some work in this field is already ongoing, and has been briefly commented on in the review. Stable and energy-preserving simulations in complex settings would eliminate the need for artificial dissipation, with a consequent more accurate representation of the flow physics in real-world applications.

References

[1] Phillips, N. A., 1959, "An Example of Nonlinear Computational Instability," *The Atmosphere and the Sea in Motion*, Rockefeller Institute Press, Oxford University Press, Oxford, UK, pp. 501–504.

[2] Lorenz, E. N., 1960, "Energy and Numerical Weather Prediction," Tellus, **12**(4), pp. 364–373.

[3] Bryan, K., 1966, "A Scheme for Numerical Integration of the Equations of Motion on an Irregular Grid Free of Nonlinear Instability," Mon. Weather Rev., **94**(1), pp. 39–40.

[4] Perot, J. B., 2011, "Discrete Conservation Properties of Unstructured Mesh Schemes," Annu. Rev. Fluid. Mech., **43**(1), pp. 299–318.

[5] Koren, B., Abgrall, R., Bochev, P., Frank, J., and Perot, B., 2013, "Physics–Compatible Numerical Methods," J. Comput. Phys., **257**(Pt B), p. 1039.

[6] Arakawa, A., 1966, "Computational Design for Long-Term Numerical Integration of the Equations of Fluid Motion: Two-Dimensional Incompressible Flow—Part I," J. Comput. Phys., **1**(1), pp. 119–143.

[7] Coppola, G., Capuano, F., and de Luca, L., 2017, "Energy-Preserving Discretizations of the Navier-Stokes Equations. Classical and Modern Approaches," XXIII Conference of the Italian Association of Theoretical and Applied Mechanics (AIMETA), Salerno, Italy, Sept. 4–7, pp. 2284–2310.

[8] Sanderse, B., and Koren, B., 2012, "Accuracy Analysis of Explicit Runge-Kutta Methods Applied to the Incompressible Navier-Stokes Equations," J. Comput. Phys., **231**(8), pp. 3041–3063.

[9] Morinishi, Y., Lund, T. S., Vasilyev, O. V., and Moin, P., 1998, "Fully Conservative Higher Order Finite Difference Schemes for Incompressible Flows," J. Comput. Phys., **143**(1), pp. 90–124.

[10] Felten, F., and Lund, T., 2006, "Kinetic Energy Conservation Issues Associated With the Collocated Mesh Scheme for Incompressible Flow," J. Comput. Phys., **215**(2), pp. 465–484.

[11] Verstappen, R. W. C. P., and Veldman, A. E. P., 2003, "Symmetry—Preserving Discretization of Turbulent Flow," J. Comput. Phys., **187**(1), pp. 343–368.

[12] Lele, S. K., 1992, "Compact Finite Difference Schemes With Spectral–Like Resolution," J. Comput. Phys., **103**(1), pp. 16–42.

[13] Horiuti, K., 1987, "Comparison of Conservative and Rotational Forms in Large Eddy Simulation of Turbulent Channel Flow," J. Comput. Phys, **71**(2), pp. 343–370.

[14] Blaisdell, G. A., Spyropoulos, E. T., and Qin, J. H., 1996, "The Effect of the Formulation of Nonlinear Terms on Aliasing Errors in Spectral Methods," Appl. Numer. Math., **21**(3), pp. 207–219.

[15] Kravhcenko, A. G., and Moin, P., 1997, "On the Effect of Numerical Errors in Large Eddy Simulations of Turbulent Flows," J. Comput. Phys., **131**, pp. 310–322.

[16] Laizet, S., and Lamballais, E., 2009, "High-Order Compact Schemes for Incompressible Flows: A Simple and Efficient Method With Quasi-Spectral Accuracy," J. Comput. Phys., **228**(16), pp. 5989–6015.

[17] Gibson, J. F., 2014, "Channel flow: A Spectral Navier-Stokes Simulator in C++," University of New Hampshire, Durham, NH.

[18] Mahesh, K., Constantinescu, G., and Moin, P., 2004, "A Numerical Method for Large-Eddy Simulation in Complex Geometries," J. Comput. Phys., **197**(1), pp. 215–240.

[19] Vallefuoco, D., Capuano, F., and Coppola, G., 2019, "Discrete Conservation of Helicity in Numerical Simulations of Incompressible Turbulent Flows," *Direct and Large-Eddy Simulation XI*, Vol. 25, Springer, Cham, Switzerland, pp. 17–22.

[20] Brachet, M. E., Meiron, D. I., Orszag, S. A., Nickel, B. G., Morf, R. H., and Frisch, U., 1983, "Small-Scale Structure of the Taylor-Green Vortex," J. Fluid Mech., **130**(1), pp. 411–452.

[21] Canuto, C., Hussaini, M., Quarteroni, A., and Zang, T., 2006, *Spectral Methods. Fundamentals in Single Domains*, Springer, Berlin.

[22] Capuano, F., Coppola, G., Balarac, G., and de Luca, L., 2015, "Energy Preserving Turbulent Simulations at a Reduced Computational Cost," J. Comput. Phys., **298**, pp. 480–494.

[23] Germano, M., Piomelli, U., Moin, P., and Cabot, W. H., 1991, "A Dynamic Subgrid-Scale Eddy Viscosity Model," Phys. Fluids A, **3**(7), pp. 1760–1765.

[24] Harlow, F., and Welch, J., 1965, "Numerical Calculation of Time-Dependent Viscous Incompressible Flow of Fluid With Free Surface," Phys. Fluids, **8**(12), pp. 2182–2189.

[25] Ham, F. E., Lien, F. S., and Strong, A. B., 2002, "A Fully Conservative Second-Order Finite Difference Scheme for Incompressible Flow on Nonuniform Grid," J. Comput. Phys., **177**(1), pp. 117–133.

[26] Feiereisen, W. J., Reynolds, W. C., and Ferziger, J. H., 1981, "Numerical Simulation of Compressible, Homogeneous Turbulent Shear Flow," Stanford University, Stanford, CA, Report No. TF-13.

[27] Kennedy, C. A., and Gruber, A., 2008, "Reduced Aliasing Formulations of the Convective Terms Within the Navier-Stokes Equations for a Compressible Fluid," J. Comput. Phys., **227**(3), pp. 1676–1700.

[28] Pirozzoli, S., 2010, "Generalized Conservative Approximations of Split Convective Derivative Operators," J. Comput. Phys., **229**(19), pp. 7180–7190.

[29] Coppola, G., Capuano, F., Pirozzoli, S., and de Luca, L., 2019, "Numerically Stable Formulations of Convective Terms for Turbulent Compressible Flows," J. Comput. Phys., **382**, pp. 86–104.

[30] Honein, A. E., and Moin, P., 2004, "Higher Entropy Conservation and Numerical Stability of Compressible Turbulence Simulations," J. Comput. Phys., **201**(2), pp. 531–545.

[31] Zang, T. A., 1991, "On the Rotation and Skew-Symmetric Forms for Incompressible Flow Simulations," Appl. Numer. Math., **7**(1), pp. 27–40.

[32] Kerr, R. M., 1985, "Higher-Order Derivative Correlations and the Alignment of Small-Scale Structures in Isotropic Numerical Turbulence," J. Fluid Mech., **153**(1), pp. 31–58.

[33] Capuano, F., Coppola, G., and de Luca, L., 2015, "An Efficient Time Advancing Strategy for Energy-Preserving Simulations," J. Comput. Phys., **295**, pp. 209–229.

[34] Capuano, F., Coppola, G., Balarac, G., Bae, H., and de Luca, L., 2014, "A Low-Cost Time-Advancing Strategy for Energy-Preserving Turbulent Simulations," *Summer Program, Center for Turbulence Research Stanford*, Stanford, CA, July 6–Aug. 1, pp. 377–386.

[35] Capuano, F., Coppola, G., and de Luca, L., 2016, "Low-Cost Energy-Preserving RK Schemes for Turbulent Simulations," *Progress in Turbulence VI: Proceedings of the iTi Conference on Turbulence 2014*, J. Peinke, G.

Kampers, M. Oberlack, M. Wacławczyk, and A. Talamelli, eds., Springer International Publishing, Cham, Switzerland, pp. 65–68.
[36] Pirozzoli, S., 2011, "Numerical Methods for High-Speed Flows," Annu. Rev. Fluid Mech., **43**(1), pp. 163–194.
[37] Kaltenbach, H.-J., and Driller, D., 2001, "LES of Wall-Bounded Turbulence Based on a 6th-Order Compact Scheme," *Direct and Large-Eddy Simulation IV* (ERCOFTAC Series, Vol. 8), B. J. Geurts, R. Friedrich, and O. Métais, eds., Springer, Dordrecht, The Netherlands, pp. 37–44.
[38] Knikker, R., 2009, "Study of a Staggered Fourth-Order Compact Scheme for Unsteady Incompressible Viscous Flows," Int. J. Numer. Methods Fluids, **59**(10), pp. 1063–1092.
[39] Vasilyev, O. V., 2000, "High Order Finite Difference Schemes on Non-Uniform Meshes With Good Conservation Properties," J. Comput. Phys., **157**(2), pp. 746–761.
[40] Verzicco, R., and Orlandi, P., 1996, "A Finite Difference Scheme for Three-Dimensional Incompressible Flows in Cylindrical Coordinates," J. Comput. Phys., **123**(2), pp. 402–414.
[41] Fukagata, K., and Kasagi, N., 2002, "Highly Energy-Conservative Finite Difference Method for the Cylindrical Coordinate System," J. Comput. Phys., **181**(2), pp. 478–498.
[42] Morinishi, Y., Vasilyev, O. V., and Ogi, T., 2004, "Fully Conservative Finite Difference Scheme in Cylindrical Coordinates for Incompressible Flow Simulations," J. Comput. Phys., **197**(2), pp. 686–710.
[43] Desjardins, O., Blanquart, G., Balarac, G., and Pitsch, H., 2008, "High Order Conservative Finite Difference Scheme for Variable Density Low Mach Number Turbulent Flows," J. Comput. Phys., **227**(15), pp. 7125–7159.
[44] Ducros, F., Laporte, F., Souleres, T., Guinot, V., Moinat, P., and Caruelle, B., 2000, "High-Order Fluxes for Conservative Skew-Symmetric-Like Schemes in Structured Meshes: Application to Compressible Flows," J. Comput. Phys., **161**(1), pp. 114–139.
[45] Kok, J. C., 2009, "A High-Order Low-Dispersion Symmetry-Preserving Finite Volume Method for Compressible Flow on Curvilinear Grids," J. Comput. Phys., **228**(18), pp. 6811–6832.
[46] Pirozzoli, S., 2011, "Stabilized Non-Dissipative Approximations of Euler Equations in Generalized Curvilinear Coordinates," J. Comput. Phys., **230**(8), pp. 2997–3014.
[47] Rozema, W., 2015, "Low-Dissipation Methods and Models for the Simulation of Turbulent Subsonic Flow: Theory and Applications," Ph.D. thesis, University of Groningen, Groningen, The Netherlands.
[48] Rozema, W., Kok, J. C., Verstappen, R. W. C. P., and Veldman, A. E. P., 2014, "A Symmetry-Preserving Discretisation and Regularisation Model for Compressible Flow With Application to Turbulent Channel Flow," J. Turbul., **15**(6), pp. 386–410.
[49] Brouwer, J., Reiss, J., and Sesterhenn, J., 2014, "Conservative Time Integrators of Arbitrary Order for Skew-Symmetric Finite Difference Discretizations of Compressible Flow," Comput. Fluids, **100**, pp. 1–12.
[50] Morinishi, Y., 2010, "Skew-Symmetric Form of Convective Terms and Fully Conservative Finite Difference Schemes for Variable Density Low-Mach Number Flows," J. Comput. Phys., **229**(2), pp. 276–300.
[51] Perot, B., 2000, "Conservation Properties of Unstructured Staggered Mesh Schemes," J. Comput. Phys., **159**(1), pp. 58–89.
[52] Zhang, X., Schmidt, D., and Perot, B., 2002, "Accuracy and Conservation Properties of a Three-Dimensional Unstructured Staggered Mesh Scheme for Fluid Dynamics," J. Comput. Phys., **175**(2), pp. 764–791.
[53] Trias, F. X., Lehmkuhl, O., Oliva, A., Pérez-Segarra, C. D., and Verstappen, R. W. C. P., 2014, "Symmetry-Preserving Discretization of Navier-Stokes Equations on Collocated Unstructured Grids," J. Comput. Phys., **258**, pp. 246–267.
[54] Modesti, D., and Pirozzoli, S., 2017, "A Low-Dissipative Solver for Turbulent Compressible Flows on Unstructured Meshes, With Openfoam Implementation," Comput. Fluids, **152**, pp. 14–23.
[55] Svärd, M., and Nordström, J., 2014, "Review of Summation-by-Parts Schemes for Initial–Boundary-Value Problems," J. Comput. Phys., **268**, pp. 17–38.
[56] Fernández, D. C. D. R., Hicken, J. E., and Zingg, D. W., 2014, "Review of Summation-by-Parts Operators With Simultaneous Approximation Terms for the Numerical Solution of Partial Differential Equations," Comput. Fluids, **95**, pp. 171–196.
[57] Sanderse, B., Verstappen, R. W. C. P., and Koren, B., 2014, "Boundary Treatment for Fourth-Order Staggered Mesh Discretizations of the Incompressible Navier–Stokes Equations," J. Comput. Phys., **257**, pp. 1472–1505.
[58] Olver, P. J., 1982, "A Nonlinear Hamiltonian Structure for the Euler Equations," J. Math. Anal. Appl., **89**(1), pp. 233–250.
[59] Moffatt, H., and Tsinober, A., 1992, "Helicity in Laminar and Turbulent Flow," Annu. Rev. Fluid Mech., **24**(1), pp. 281–312.
[60] Palha, A., and Gerritsma, M., 2017, "A Mass, Energy, Enstrophy and Vorticity Conserving (MEEVC) Mimetic Spectral Element Discretization for the 2D Incompressible Navier–Stokes Equations," J. Comput. Phys., **328**, pp. 200–220.
[61] Lee, D., Palha, A., and Gerritsma, M., 2017, "Discrete Conservation Properties for Shallow Water Flows Using Mixed Mimetic Spectral Elements," J. Comput. Phys., **357**, pp. 282–304.
[62] Liu, J.-G., and Wang, W.-C., 2004, "Energy and Helicity Preserving Schemes for Hydro- and Magnetohydro-Dynamics Flows With Symmetry," J. Comput. Phys., **200**(1), pp. 8–33.
[63] Rebholz, L. G., 2007, "An Energy- and Helicity-Conserving Finite Element Scheme for the Navier-Stokes Equations," SIAM J. Numer. Anal., **45**(4), pp. 1622–1638.
[64] Olshanskii, M. A., and Rebholz, L. G., 2010, "Velocity–Vorticity–Helicity Formulation and a Solver for the Navier–Stokes Equations," J. Comput. Phys., **229**(11), pp. 4291–4303.
[65] Olshanskii, M., and Rebholz, L. G., 2010, "Note on Helicity Balance of the Galerkin Method for the 3D Navier–Stokes Equations," Comput. Methods Appl. Mech. Eng., **199**(17–20), pp. 1032–1035.
[66] Capuano, F., and Vallefuoco, D., 2018, "Effects of Discrete Energy and Helicity Conservation in Numerical Simulations of Helical Turbulence," Flow Turbul. Combust., **101**(2), pp. 343–364.
[67] Fuster, D., 2013, "An Energy Preserving Formulation for the Simulation of Multiphase Turbulent Flows," J. Comput. Phys., **235**, pp. 114–128.
[68] Morinishi, Y., and Koga, K., 2014, "Skew-Symmetric Convection Form and Secondary Conservative Finite Difference Methods for Moving Grids," J. Comput. Phys., **257**, pp. 1081–1112.
[69] Charnyi, S., Heister, T., Olshanskii, M. A., and Rebholz, L. G., 2017, "On Conservation Laws of Navier–Stokes Galerkin Discretizations," J. Comput. Phys., **337**, pp. 289–308.
[70] Pastrana, D., Cajas, J., Lehmkuhl, O., Rodríguez, I., and Houzeaux, G., 2018, "Large-Eddy Simulations of the Vortex-Induced Vibration of a Low Mass Ratio Two-Degree-of-Freedom Circular Cylinder at Subcritical Reynolds Numbers," Comput. Fluids, **173**, pp. 118–132.
[71] Moura, R., Mengaldo, G., Peirò, J., and Sherwin, S., 2017, "On the Eddy-Resolving Capability of High-Order Discontinuous Galerkin Approaches to Implicit LES/Under-Resolved DNS of Euler Turbulence," J. Comput. Phys., **330**, pp. 615–623.
[72] Gassner, G. J., Winters, A. R., and Kopriva, D. A., 2016, "Split Form Nodal Discontinuous Galerkin Schemes With Summation-by-Parts Property for the Compressible Euler Equations," J. Comput. Phys., **327**, pp. 39–66.
[73] Gassner, G. J., 2014, "A Kinetic Energy Preserving Nodal Discontinuous Galerkin Spectral Element Method," Int. J. Numer. Methods Fluids, **76**(1), pp. 28–50.
[74] Winters, A. R., Moura, R. C., Mengaldo, G., Gassner, G. J., Walch, S., Peiro, J., and Sherwin, S. J., 2018, "A Comparative Study on Polynomial Dealiasing and Split Form Discontinuous Galerkin Schemes for Under-Resolved Turbulence Computations," J. Comput. Phys., **372**, pp. 1–21.
[75] Capuano, F., Coppola, G., Chiatto, M., and de Luca, L., 2016, "Approximate Projection Method for the Incompressible Navier-Stokes Equations," AIAA J., **54**(7), pp. 2178–2181.
[76] Rosenbaum, J., 1976, "Conservation Properties of Numerical Integration Methods for Systems of Ordinary Differential Equations," J. Comput. Phys., **20**(3), pp. 259–267.
[77] Iserles, A., and Zanna, A., 2000, "Solving ODEs Numerically While Preserving a First Integral," J. Comput. Appl. Math., **125**(1–2), pp. 69–81.
[78] Hairer, E., Lubich, C., and Wanner, G., 2006, *Geometric Numerical Integration*, Springer, Berlin.
[79] Rogallo, R. S., and Moin, P., 1984, "Numerical Simulation of Turbulent Flows," Annu. Rev. Fluid. Mech., **16**(1), pp. 99–137.
[80] Orlandi, P., 2000, *Fluid Flow Phenomena: A Numerical Toolkit*, Springer, Dordrecht, The Netherlands.
[81] Griffiths, D. F., and Higham, D. J., 2010, *Numerical Methods for Ordinary Differential Equations*, Springer, London.
[82] Le, H., and Moin, P., 1991, "An Improvement of Fractional Step Methods for the Incompressible Navier-Stokes Equations," J. Comput. Phys., **92**(2), pp. 369–379.
[83] Butcher, J. C., 2004, *Numerical Methods for Ordinary Differential Equations*, Wiley, Hoboken, NJ.
[84] Sanz-Serna, J. M., 1988, "Runge-Kutta Schemes for Hamiltonian Systems," BIT, **28**(4), pp. 877–883.
[85] Sanderse, B., 2013, "Energy Conserving Runge-Kutta Methods for the Incompressible Navier-Stokes Equations," J. Comput. Phys., **233**, pp. 100–131.
[86] Duponcheel, M., Orlandi, P., and Winckelmans, G., 2008, "Time-Reversibility of the Euler Equations as a Benchmark for Energy Conserving Schemes," J. Comput. Phys., **227**(19), pp. 8736–8752.
[87] Verstappen, R. W. C. P., and Veldman, A. E. P., 1997, "Direct Numerical Simulation of Turbulence at Lower Costs," J. Eng. Math., **32**(2/3), pp. 143–159.
[88] Aubry, A., and Chartier, P., 1998, "Pseudo-Symplectic Runge-Kutta Methods," BIT Numer. Math., **38**(3), pp. 439–461.
[89] Capuano, F., Coppola, G., Rández, L., and de Luca, L., 2017, "Explicit Runge-Kutta Schemes for Incompressible Flow With Improved Energy-Conservation Properties," J. Comput. Phys., **328**, pp. 86–94.
[90] Calvo, M., Laburta, M., Montijano, J., and Rández, L., 2010, "Approximate Preservation of Quadratic First Integrals by Explicit Runge-Kutta Methods," Adv. Comput. Math., **32**(3), pp. 255–274.
[91] Capuano, F., De Angelis, E. M., Coppola, G., and de Luca, L., 2019, "An Analysis of Time-Integration Errors in Large-Eddy Simulation of Incompressible Turbulent Flows," *Direct and Large-Eddy Simulation XI*, M. Salvetti, V. Armenio, J. Fröhlich, B. Geurts, and H. Kuerten, eds., Vol. 25, Springer, Cham, Switzerland, pp. 31–37.
[92] Capuano, F., Sanderse, B., De Angelis, E. M., and Coppola, G., 2017, "A Minimum-Dissipation Time-Integration Strategy for Large-Eddy Simulation of Incompressible Turbulent Flows," XXIII Conference of the Italian Association of Theoretical and Applied Mechanics (AIMETA), Salerno, Italy, Sept. 4–7, pp. 2311–2323.
[93] Gottlieb, S., Shu, C.-W., and Tadmor, E., 2001, "Strong Stability-Preserving High-Order Time Discretization Methods," SIAM Rev., **43**(1), pp. 89–112.
[94] Hu, F., Hussaini, M., and Manthey, J., 1996, "Low-Dissipation and Low-Dispersion Runge–Kutta Schemes for Computational Acoustics," J. Comput. Phys., **124**(1), pp. 177–191.

[95] Colonius, T., and Lele, S. K., 2004, "Computational Aeroacoustics: Progress on Nonlinear Problems of Sound Generation," Prog. Aerosp. Sci., **40**(6), pp. 345–416.
[96] Subbareddy, P. K., and Candler, G. V., 2009, "A Fully Discrete, Kinetic Energy Consistent Finite Volume Scheme for Compressible Flows," J. Comput. Phys., **228**(5), pp. 1347–1364.
[97] Canuto, C., Hussaini, M., Quarteroni, A., and Zang, T., 2007, *Spectral Methods. Evolution to Complex Geometries and Applications to Fluid Dynamics*, Springer, Berlin.
[98] Cook, A. W., and Cabot, W. H., 2004, "A High-Wavenumber Viscosity for High-Resolution Numerical Methods," J. Comput. Phys., **195**(2), pp. 594–601.
[99] Kawai, S., and Lele, S. K., 2008, "Localized Artificial Diffusivity Scheme for Discontinuity Capturing on Curvilinear Meshes," J. Comput. Phys., **227**(22), pp. 9498–9526.
[100] Visbal, M. R., and Gaitonde, D. V., 2002, "On the Use of Higher-Order Finite Difference Schemes on Curvilinear and Deforming Meshes," J. Comput. Phys., **181**(1), pp. 155–185.
[101] Visbal, M. R., and Rizzetta, D., 2002, "Large-Eddy Simulation on Curvilinear Grids Using Compact Differencing and Filtering Schemes," ASME J. Fluids Eng., **124**(4), pp. 836–847.
[102] Mittal, R., and Moin, P., 1997, "Suitability of Upwind–Biased Finite Difference Schemes for Large–Eddy Simulation of Turbulent Flows," AIAA J., **35**, pp. 1415–1417.
[103] Ghosal, S., 1996, "An Analysis of Numerical Errors in Large-Eddy Simulations of Turbulence," J. Comput. Phys., **125**(1), pp. 187–206.
[104] You, D., Ham, F., and Moin, P., 2008, "Discrete Conservation Principles in Large-Eddy Simulation With Application to Separation Control Over an Airfoil," Phys. Fluids, **20**(10), p. 101515.
[105] Davidson, L., Cokljat, D., Fröhlich, J., Leschziner, M. A., Mellen, C., and Rodi, W., 2003, *LESFOIL: Large Eddy Simulation of Flow Around a High Lift Airfoil: Results of the Project LESFOIL Supported by the European Union 1998–2001*, Vol. 83, Springer Science & Business Media, Berlin.
[106] Schmitt, V., 1979, "Pressure Distributions on the Onera M6-Wing at Transonic Mach Numbers, Experimental Data Base for Computer Program Assessment," Advisory Group for Aerospace Research and Development, Neuilly-sur-Seine, France, Report No. AGARD-AR-138.
[107] Liou, M.-S., and Steffen, C. J., Jr., 1993, "A New Flux Splitting Scheme," J. Comput. Phys., **107**(1), pp. 23–39.
[108] Ducros, F., Ferrand, V., Nicoud, F., Weber, C., Darracq, D., Gacherieu, C., and Poinsot, T., 1999, "Large-Eddy Simulation of the Shock/Turbulence Interaction," J. Comput. Phys., **152**(2), pp. 517–549.
[109] Weller, H. G., Tabor, G., Jasak, H., and Fureby, C., 1998, "A Tensorial Approach to Computational Continuum Mechanics Using Object-Oriented Techniques," Comput. Phys., **12**(6), pp. 620–631.
[110] Kurganov, A., and Tadmor, E., 2000, "New High-Resolution Central Schemes for Nonlinear Conservation Laws and Convection–Diffusion Equations," J. Comput. Phys., **160**(1), pp. 241–282.
[111] Aljure, D., Lehmkuhl, O., Rodríguez, I., and Oliva, A., 2014, "Flow and Turbulent Structures Around Simplified Car Models," Comput. Fluids, **96**, pp. 122–135.
[112] Aljure, D., Calafell, J., Baez, A., and Oliva, A., 2018, "Flow Over a Realistic Car Model: Wall Modeled Large Eddy Simulations Assessment and Unsteady Effects," J. Wind Eng. Ind. Aerod., **174**, pp. 225–240.
[113] Rodríguez, I., Lehmkuhl, O., Borrell, R., and Oliva, A., 2013, "Direct Numerical Simulation of a NACA0012 in Full Stall," Int. J. Heat Fluid Flow, **43**, pp. 194–203.
[114] Lehmkuhl, O., Rodríguez, I., Borrell, R., and Oliva, A., 2013, "Low-Frequency Unsteadiness in the Vortex Formation Region of a Circular Cylinder," Phys. Fluids, **25**(8), p. 085109.
[115] Rozema, W., Kok, J. C., Verstappen, R. W. C. P., and Veldman, A. E. P., 2014, "DNS and LES of the Compressible Flow Over a Delta Wing With the Symmetry-Preserving Discretization," ASME Paper No. FEDSM2014-21374.
[116] Pitsch, H., 2006, "Large-Eddy Simulation of Turbulent Combustion," Annu. Rev. Fluid Mech., **38**(1), pp. 453–482.
[117] Selle, L., Lartigue, G., Poinsot, T., Koch, R., Schildmacher, K.-U., Krebs, W., Prade, B., Kaufmann, P., and Veynante, D., 2004, "Compressible Large Eddy Simulation of Turbulent Combustion in Complex Geometry on Unstructured Meshes," Combust. Flame, **137**(4), pp. 489–505.
[118] Ham, F., and Iaccarino, G., 2004, "Energy Conservation in Collocated Discretization Schemes on Unstructured Meshes," Annual Research Briefs 2004, Center for Turbulence Research, Stanford University, Stanford, CA, pp. 3–14.
[119] Mahesh, K., Constantinescu, G., Apte, S., Iaccarino, G., Ham, F., and Moin, P., 2006, "Large-Eddy Simulation of Reacting Turbulent Flows in Complex Geometries," ASME J. Appl. Mech., **73**(3), pp. 374–381.
[120] Sitcom-b, 2018, "SiTCom-B," accessed Feb. 27, 2019, https://www.coria-cfd.fr/index.php/SiTCom-B
[121] Domingo, P., Vervisch, L., and Veynante, D., 2008, "Large-Eddy Simulation of a Lifted Methane Jet Flame in a Vitiated Coflow," Combust. Flame, **152**(3), pp. 415–432.
[122] Petit, X., Ribert, G., Lartigue, G., and Domingo, P., 2013, "Large-Eddy Simulation of Supercritical Fluid Injection," J. Supercrit. Fluids, **84**, pp. 61–73.
[123] Vuorinen, V., Keskinen, J.-P., Duwig, C., and Boersma, B., 2014, "On the Implementation of Low-Dissipative Runge-Kutta Projection Methods for Time Dependent Flows Using OpenFOAM®," Comput. Fluids, **93**, pp. 153–163.
[124] D'Alessandro, V., Zoppi, A., Binci, L., and Ricci, R., 2016, "Development of OpenFOAM Solvers for Incompressible Navier–Stokes Equations Based on High-Order Runge-Kutta Schemes," Int. J. Comput. Methods Exp. Meas., **4**(4), pp. 594–603.